

Methods of chaos detection

Haris Skokos

**Department of Mathematics and Applied Mathematics
University of Cape Town
Cape Town, South Africa**

E-mail: haris.skokos@uct.ac.za

URL: http://math_research.uct.ac.za/~hskokos/

Outline

- **Dynamical Systems**
 - ✓ Hamiltonian models – Variational equations
 - ✓ Symplectic maps – Tangent map
- **Brief description of chaos detection methods**
- **Chaos Indicators**
 - ✓ Lyapunov exponents
 - ✓ Smaller ALignment Index – SALI
 - Definition
 - Behavior for chaotic and regular motion
 - Applications
 - ✓ Generalized ALignment Index – GALI
 - Definition - Relation to SALI
 - Behavior for chaotic and regular motion
 - Application to time-dependent models

Autonomous Hamiltonian systems

Consider an **N degree of freedom** autonomous Hamiltonian system having a Hamiltonian function of the form:

$$H(\underbrace{q_1, q_2, \dots, q_N}_{\text{positions}}, \underbrace{p_1, p_2, \dots, p_N}_{\text{momenta}})$$

The time evolution of an orbit (trajectory) with initial condition

$$P(0) = (q_1(0), q_2(0), \dots, q_N(0), p_1(0), p_2(0), \dots, p_N(0))$$

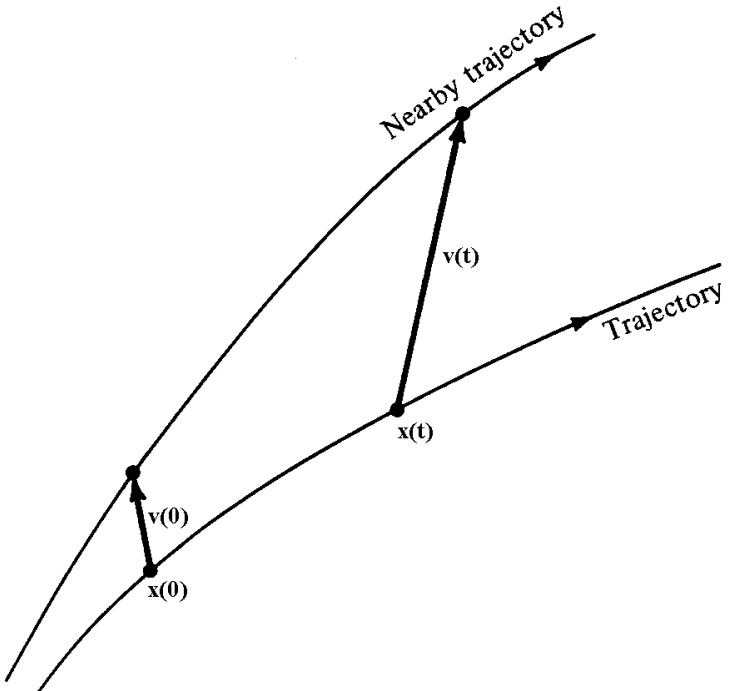
is governed by the **Hamilton's equations of motion**

$$\frac{dp_i}{dt} = -\frac{\partial H}{\partial q_i}, \quad \frac{dq_i}{dt} = \frac{\partial H}{\partial p_i}$$

Variational Equations

We use the notation $\mathbf{x} = (q_1, q_2, \dots, q_N, p_1, p_2, \dots, p_N)^T$. The **deviation vector** from a given orbit is denoted by

$$\mathbf{v} = (\delta x_1, \delta x_2, \dots, \delta x_n)^T, \text{ with } n=2N$$



The time evolution of \mathbf{v} is given by the so-called **variational equations**:

$$\frac{d\mathbf{v}}{dt} = -\mathbf{J} \cdot \mathbf{P} \cdot \mathbf{v}$$

where

$$\mathbf{J} = \begin{pmatrix} \mathbf{0}_N & -\mathbf{I}_N \\ \mathbf{I}_N & \mathbf{0}_N \end{pmatrix}, \quad \mathbf{P}_{ij} = \frac{\partial^2 H}{\partial x_i \partial x_j} \quad i, j = 1, 2, \dots, n$$

Symplectic Maps

Consider an **2N-dimensional symplectic map T**. In this case we have **discrete time**.

The evolution of an **orbit** with initial condition

$$P(0) = (x_1(0), x_2(0), \dots, x_{2N}(0))$$

is governed by the **equations of map T**

$$P(i+1) = T P(i) , i=0,1,2,\dots$$

The evolution of an initial **deviation vector**

$$v(0) = (\delta x_1(0), \delta x_2(0), \dots, \delta x_{2N}(0))$$

is given by the corresponding **tangent map**

$$v(i+1) = \left. \frac{\partial T}{\partial P} \right|_i \cdot v(i) , i = 0, 1, 2, \dots$$

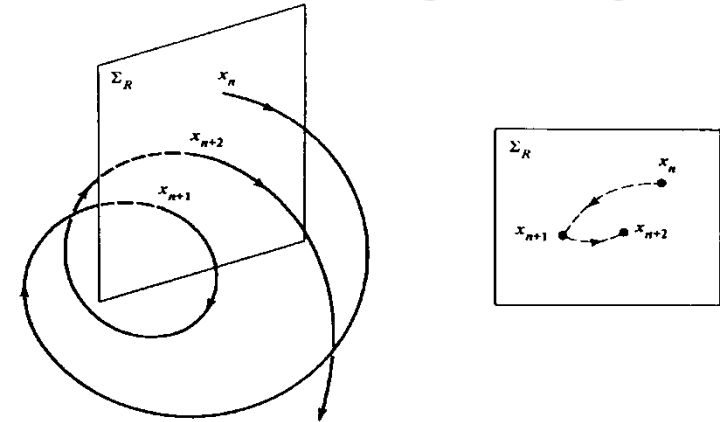
Chaos detection techniques

- Based on the visualization of orbits
 - ✓ Poincaré Surface of Section (PSS)
 - ✓ the color and rotation (CR) method
 - ✓ the 3D phase space slices (3PSS) technique

Poincaré Surface of Section (PSS)

We can constrain the study of an $N+1$ degree of freedom Hamiltonian system to a **2N-dimensional subspace of the general phase space**.

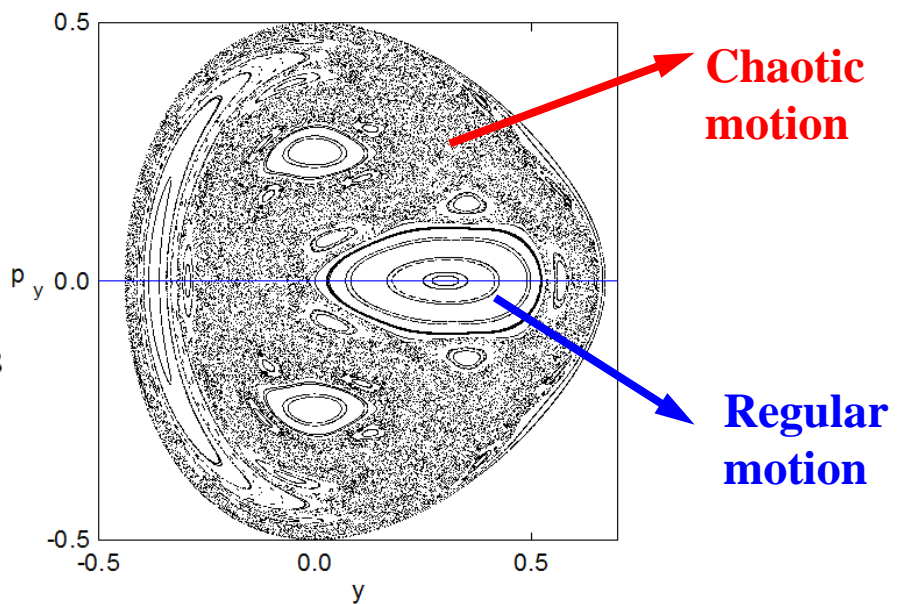
In this sense **an $N+1$ degree of freedom Hamiltonian system corresponds to a 2N-dimensional symplectic map.**



Lieberman & Lichtenberg, 1992, *Regular and Chaotic Dynamics*, Springer.

The 2D Hénon-Heiles system:

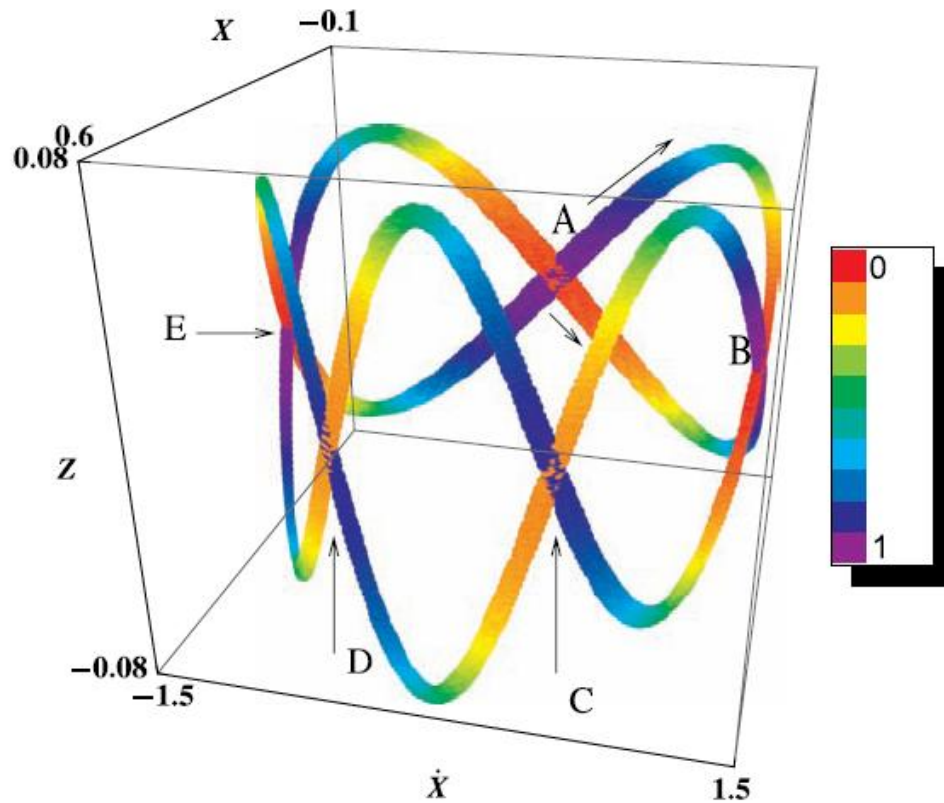
$$H_2 = \frac{1}{2}(p_x^2 + p_y^2) + \frac{1}{2}(x^2 + y^2) + x^2y - \frac{1}{3}y^3$$



The color and rotation (CR) method

For 3 degree of freedom Hamiltonian systems and 4 dimensional symplectic maps:

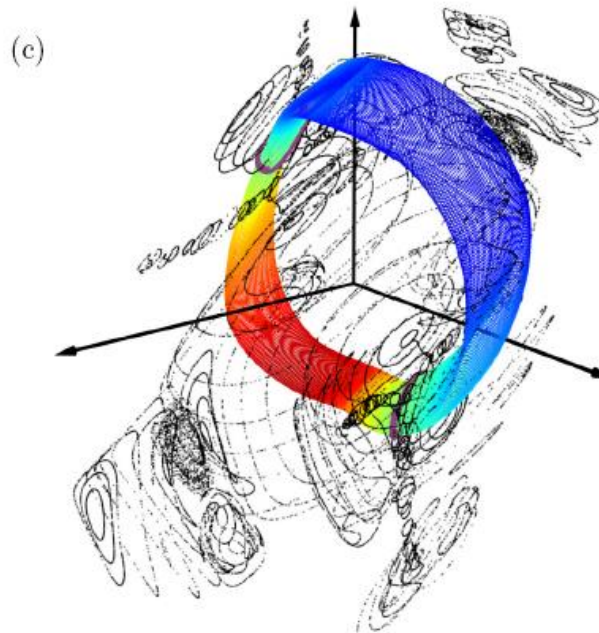
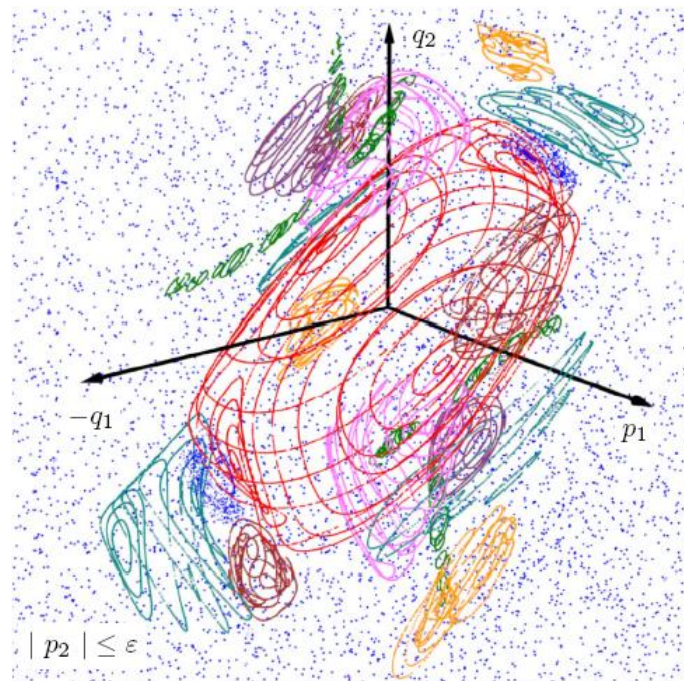
We consider the 3D projection of the PSS and use color to indicate the 4th dimension.



The 3D phase space slices (3PSS) technique

For 3 degree of freedom Hamiltonian systems and 4 dimensional symplectic maps:

We consider thin 3D phase space slices of the 4D phase space (e.g. $|p_2| \leq \varepsilon$) and present intersections of orbits with these slices.



Chaos detection techniques

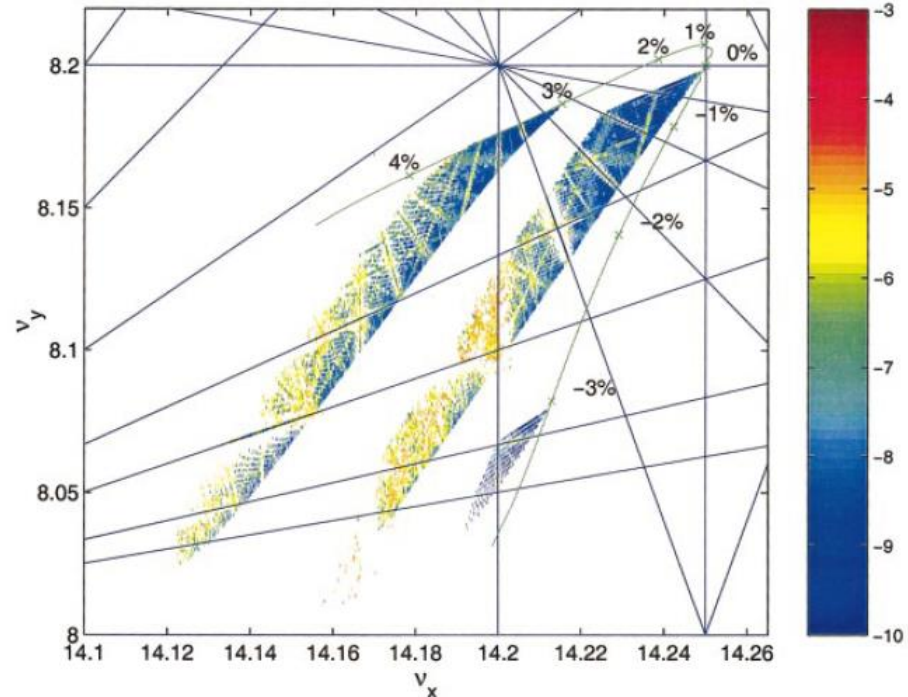
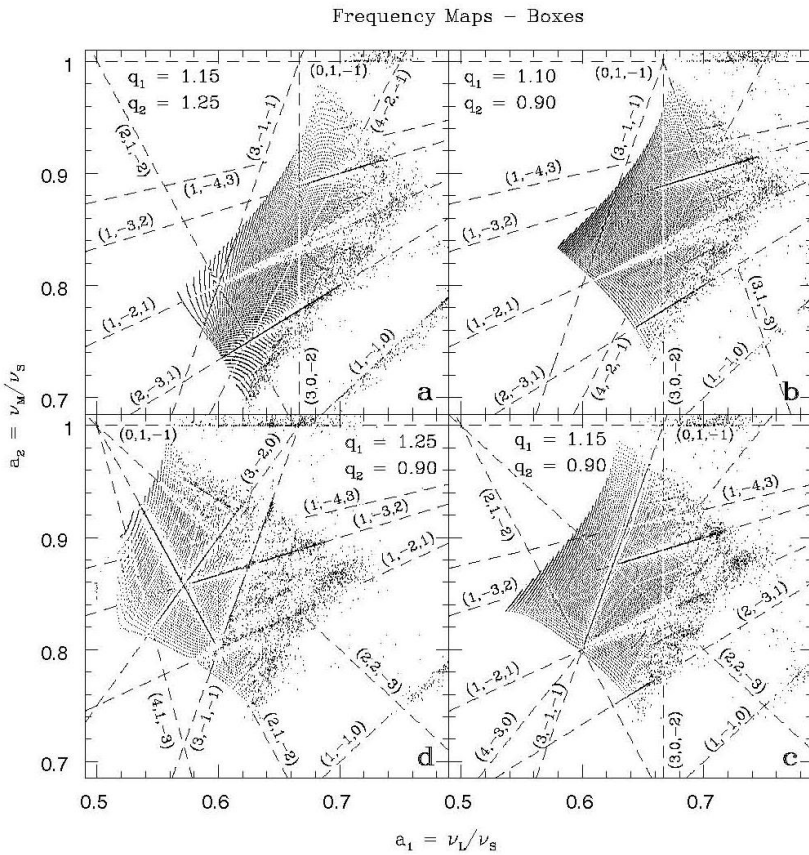
- Based on the visualization of orbits
 - ✓ Poincaré Surface of Section (PSS)
 - ✓ the color and rotation (CR) method
 - ✓ the 3D phase space slices (3PSS) technique
- Based on the numerical analysis of orbits
 - ✓ Frequency Map Analysis
 - ✓ 0-1 test

Frequency Map Analysis

Create **Frequency Maps** by computing the fundamental frequencies of orbits.

Regular motion: The computed frequencies do not vary in time

Chaotic motion: The computed frequencies vary in time



Steier C et al. 2002 Phys. Rev. E 65 056506

Chaos detection techniques

- Based on the visualization of orbits
 - ✓ Poincaré Surface of Section (PSS)
 - ✓ the color and rotation (CR) method
 - ✓ the 3D phase space slices (3PSS) technique
- Based on the numerical analysis of orbits
 - ✓ Frequency Map Analysis
 - ✓ 0-1 test
- Chaos indicators based on the evolution of deviation vectors from a given orbit
 - ✓ Maximum Lyapunov Exponent
 - ✓ Fast Lyapunov Indicator (FLI) and Orthogonal Fast Lyapunov Indicators (OFLI and OFLI2)
 - ✓ Mean Exponential Growth Factor of Nearby Orbits (MEGNO)
 - ✓ Relative Lyapunov Indicator (RLI)
 - ✓ Smaller ALignment Index – SALI
 - ✓ Generalized ALignment Index – GALI

Maximum Lyapunov Exponent

Roughly speaking, the Lyapunov exponents of a given orbit characterize the **mean exponential rate of divergence** of trajectories surrounding it.

Consider an orbit in the $2N$ -dimensional phase space with **initial condition** $\mathbf{x}(0)$ and an **initial deviation vector from it** $\mathbf{v}(0)$. Then the mean exponential rate of divergence is:

$$mLCE = \sigma_1 = \lim_{t \rightarrow \infty} \frac{1}{t} \ln \frac{\|\vec{v}(t)\|}{\|\vec{v}(0)\|}$$

$\sigma_1=0 \rightarrow$ Regular motion
 $\sigma_1 \neq 0 \rightarrow$ Chaotic motion

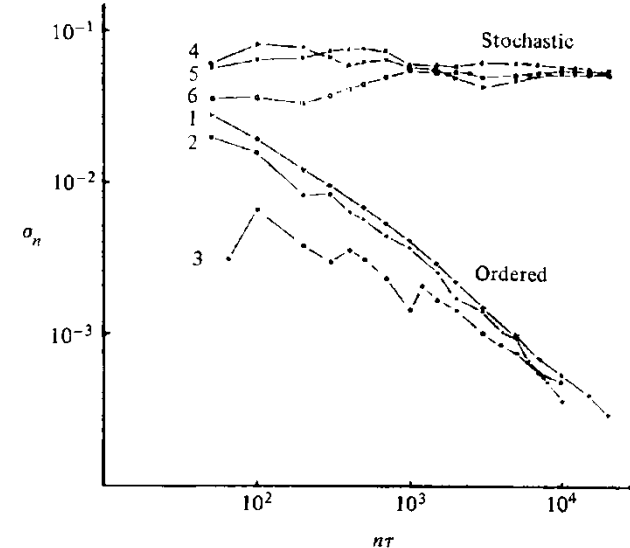


Figure 5.7. Behavior of σ_n at the intermediate energy $E = 0.125$ for initial points taken in the ordered (curves 1-3) or stochastic (curves 4-6) regions (after Benettin et al., 1976).

If we start with more than one linearly independent deviation vectors they will **align to the direction defined by the largest Lyapunov exponent** for chaotic orbits.

The
Smaller ALignment Index
(SALI)
method

Definition of the SALI

We follow the evolution in time of two different initial deviation vectors ($v_1(0)$, $v_2(0)$), and define the SALI (Ch.S. 2001, J. Phys. A) as:

$$\text{SALI}(t) = \min \left\{ \left\| \hat{v}_1(t) + \hat{v}_2(t) \right\|, \left\| \hat{v}_1(t) \cdot \hat{v}_2(t) \right\| \right\}$$

where

$$\hat{v}_1(t) = \frac{v_1(t)}{\|v_1(t)\|}$$

When the two vectors become **collinear**

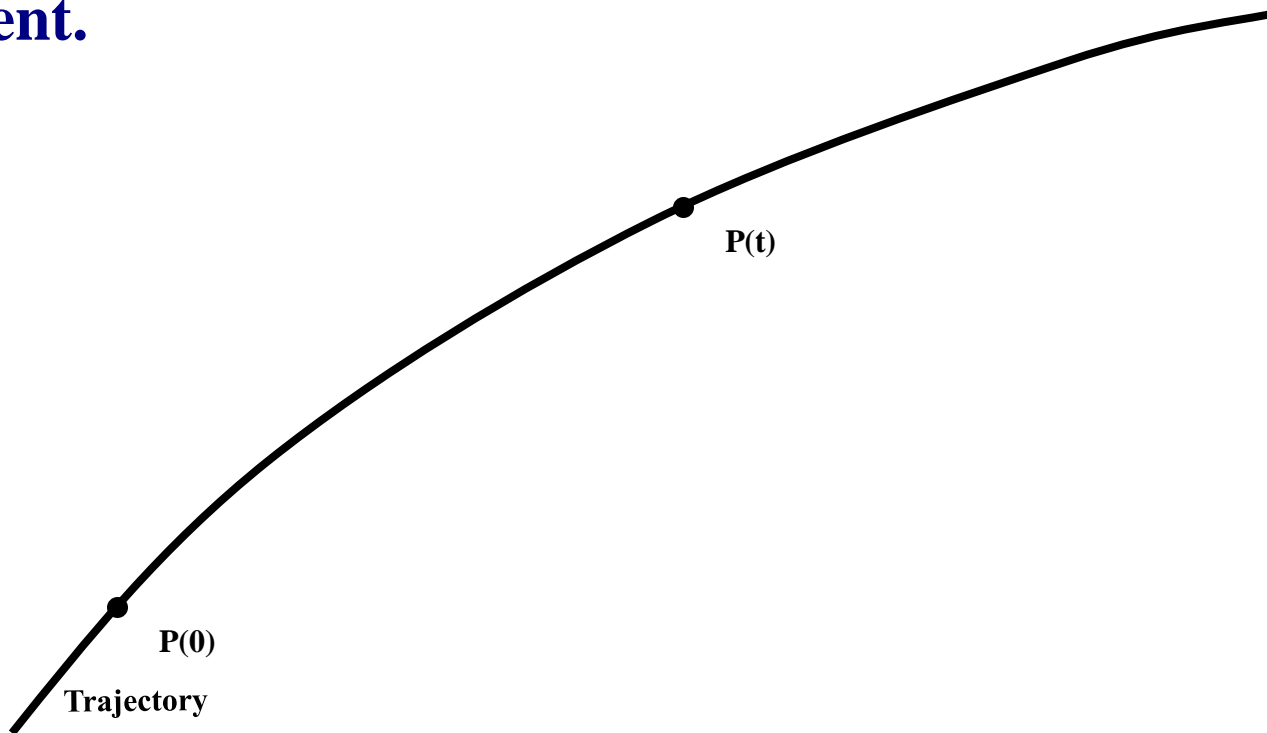
$$\text{SALI}(t) \rightarrow 0$$

Behavior of the SALI for chaotic motion

For chaotic orbits the two initially different deviation vectors tend to coincide with the direction defined by the maximum Lyapunov exponent.

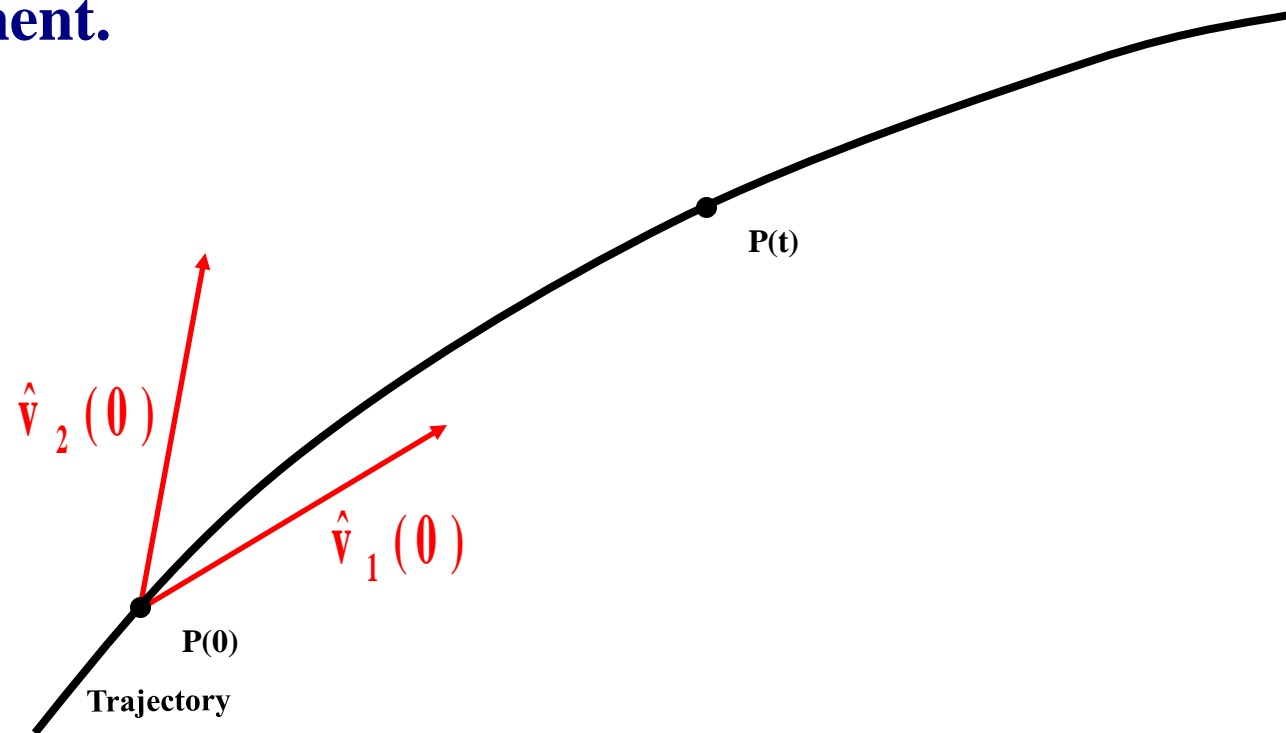
Behavior of the SALI for chaotic motion

For chaotic orbits the two initially different deviation vectors tend to coincide with the direction defined by the maximum Lyapunov exponent.



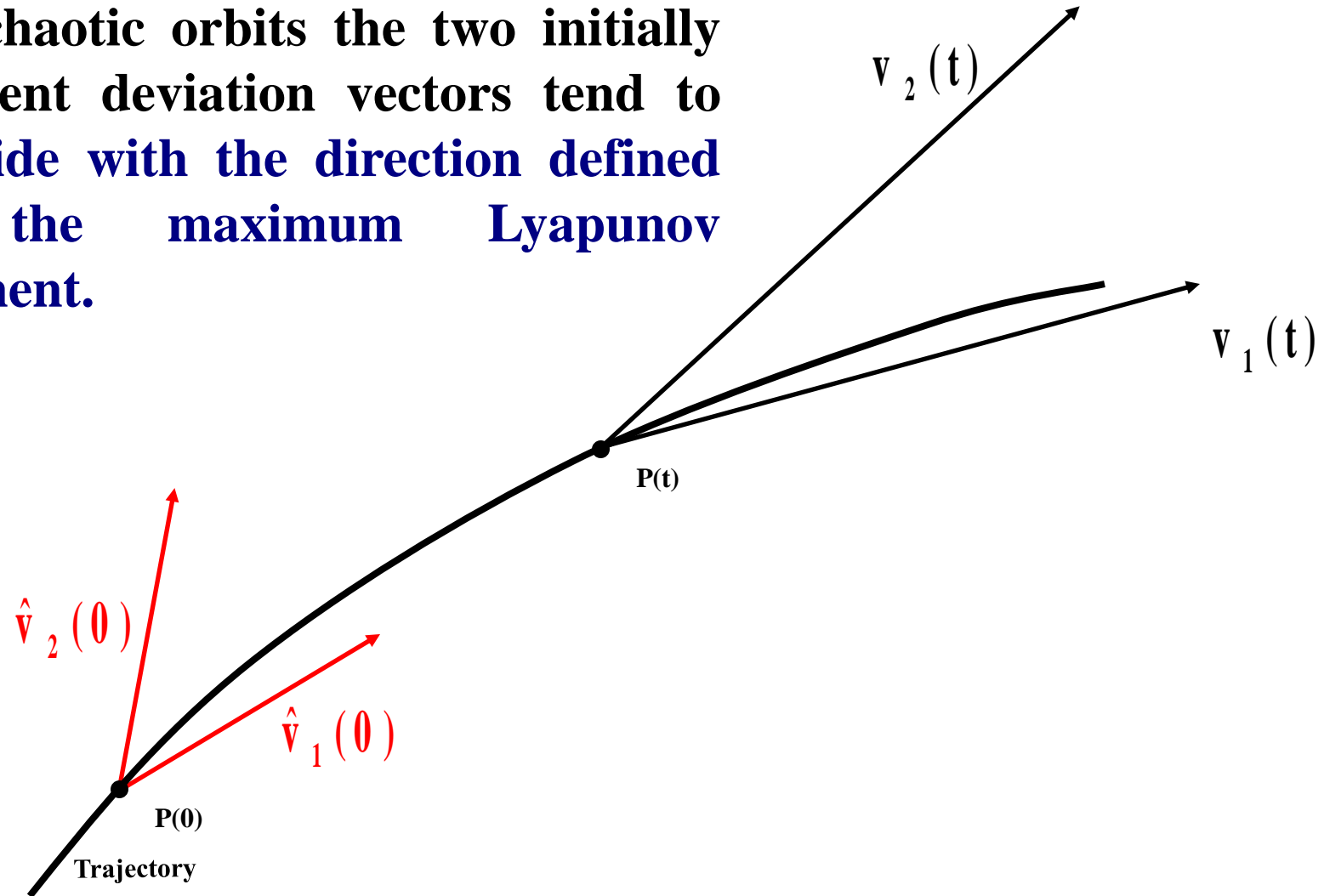
Behavior of the SALI for chaotic motion

For chaotic orbits the two initially different deviation vectors tend to coincide with the direction defined by the maximum Lyapunov exponent.



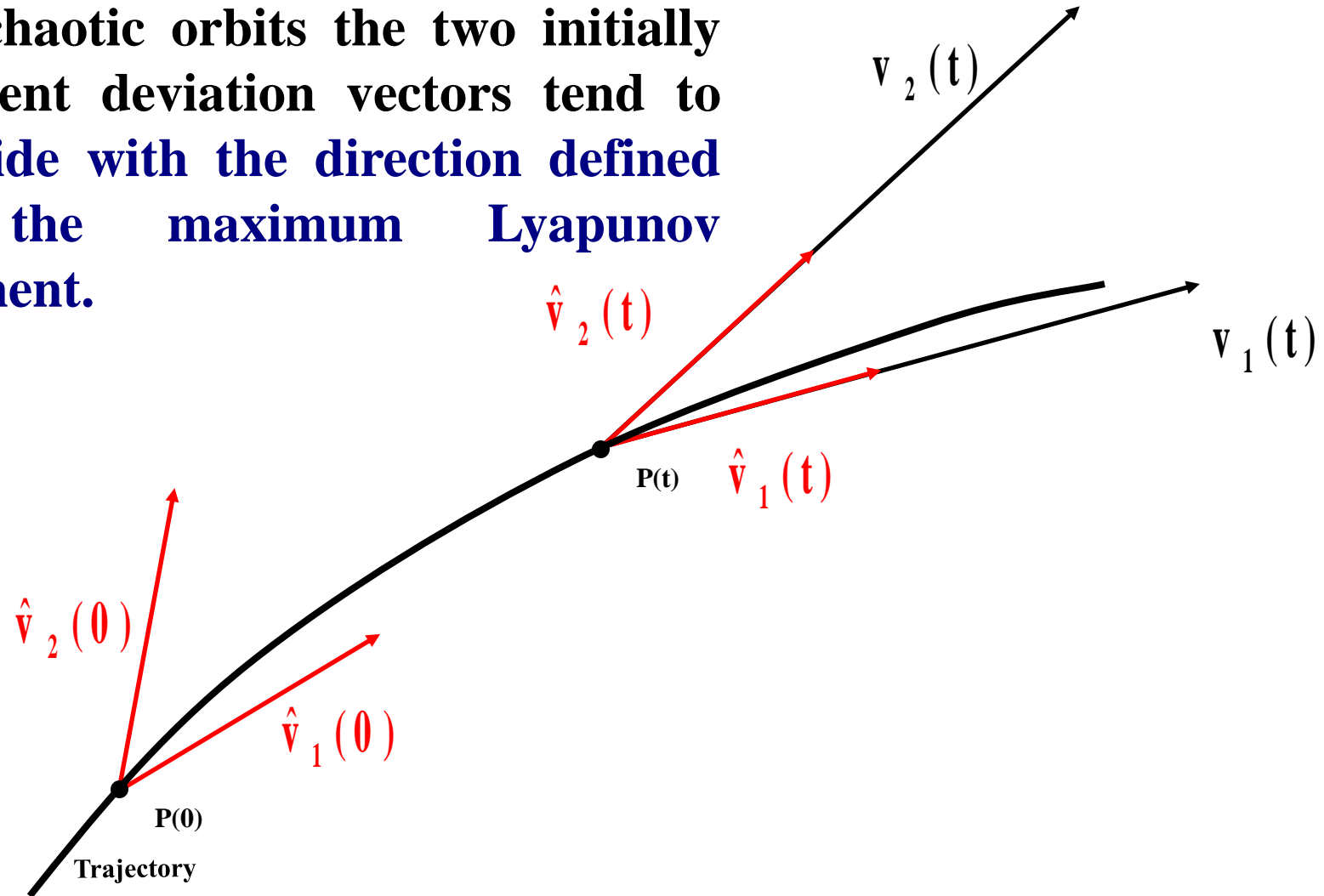
Behavior of the SALI for chaotic motion

For chaotic orbits the two initially different deviation vectors tend to coincide with the direction defined by the maximum Lyapunov exponent.



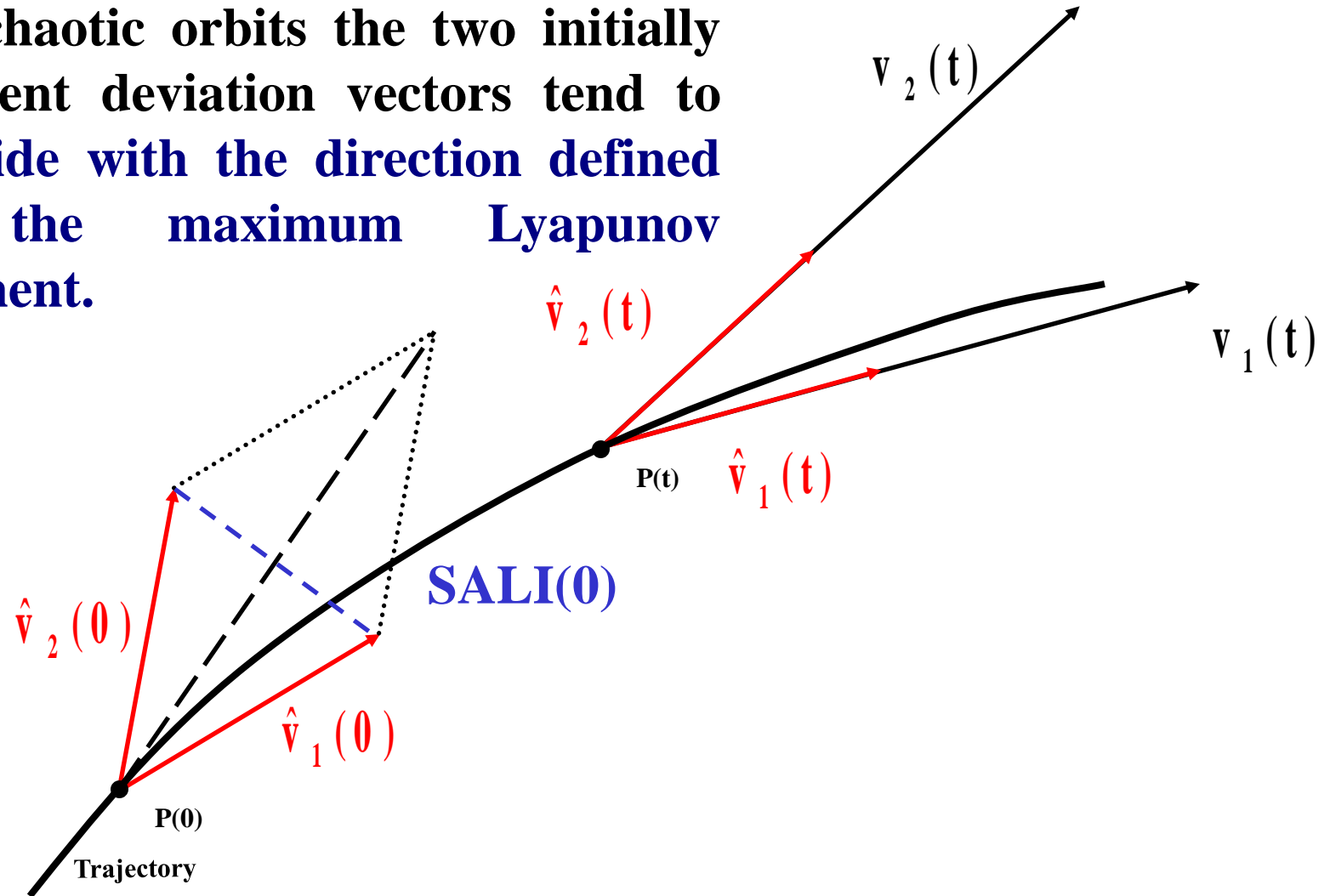
Behavior of the SALI for chaotic motion

For chaotic orbits the two initially different deviation vectors tend to coincide with the direction defined by the maximum Lyapunov exponent.



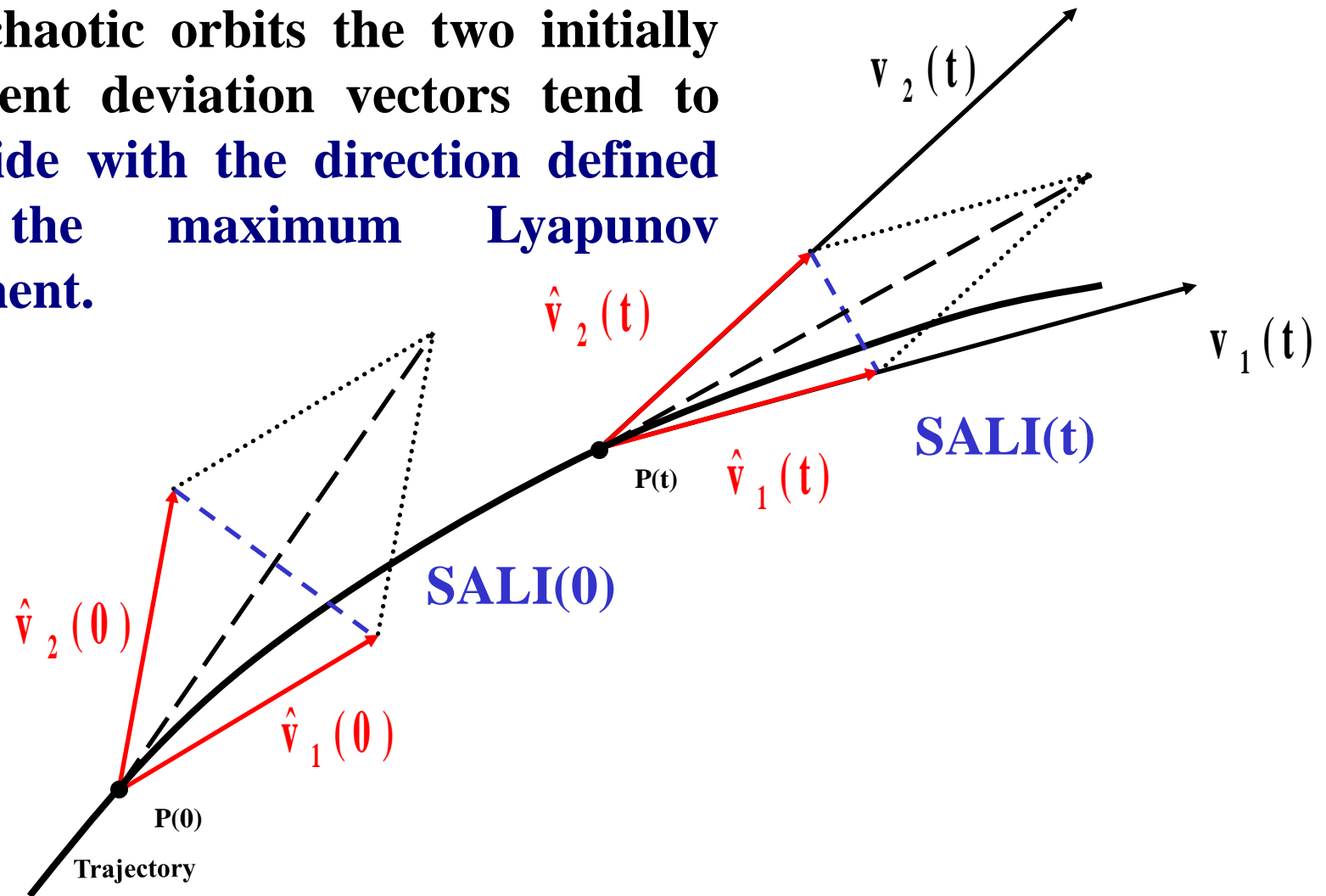
Behavior of the SALI for chaotic motion

For chaotic orbits the two initially different deviation vectors tend to coincide with the direction defined by the maximum Lyapunov exponent.



Behavior of the SALI for chaotic motion

For chaotic orbits the two initially different deviation vectors tend to coincide with the direction defined by the maximum Lyapunov exponent.

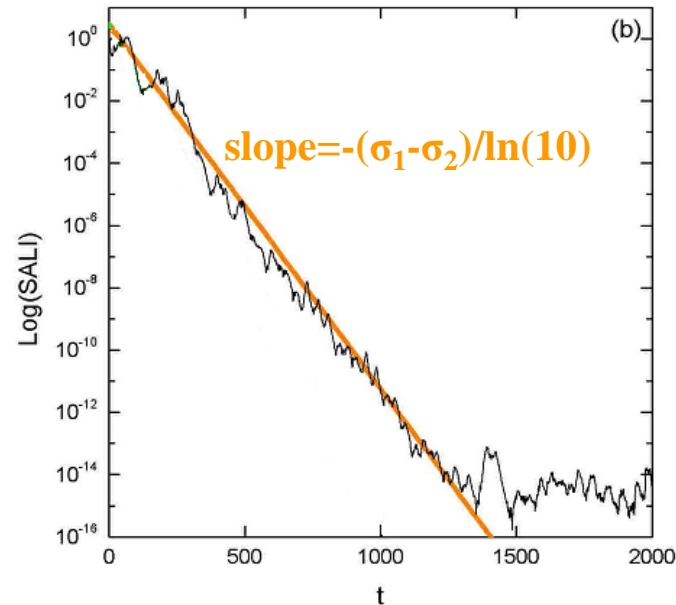
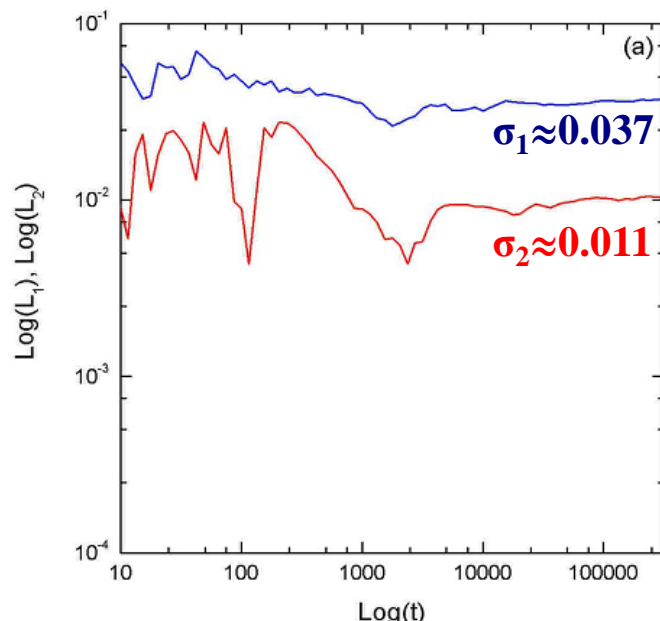


Behavior of the SALI for chaotic motion

We test the validity of the approximation $\text{SALI} \propto e^{-(\sigma_1 - \sigma_2)t}$ (Ch.S., Antonopoulos, Bountis, Vrahatis, 2004, J. Phys. A) for a chaotic orbit of the 3D Hamiltonian

$$H = \sum_{i=1}^3 \frac{\omega_i}{2} (q_i^2 + p_i^2) + q_1^2 q_2 + q_1^2 q_3$$

with $\omega_1=1$, $\omega_2=1.4142$, $\omega_3=1.7321$, $H=0.09$

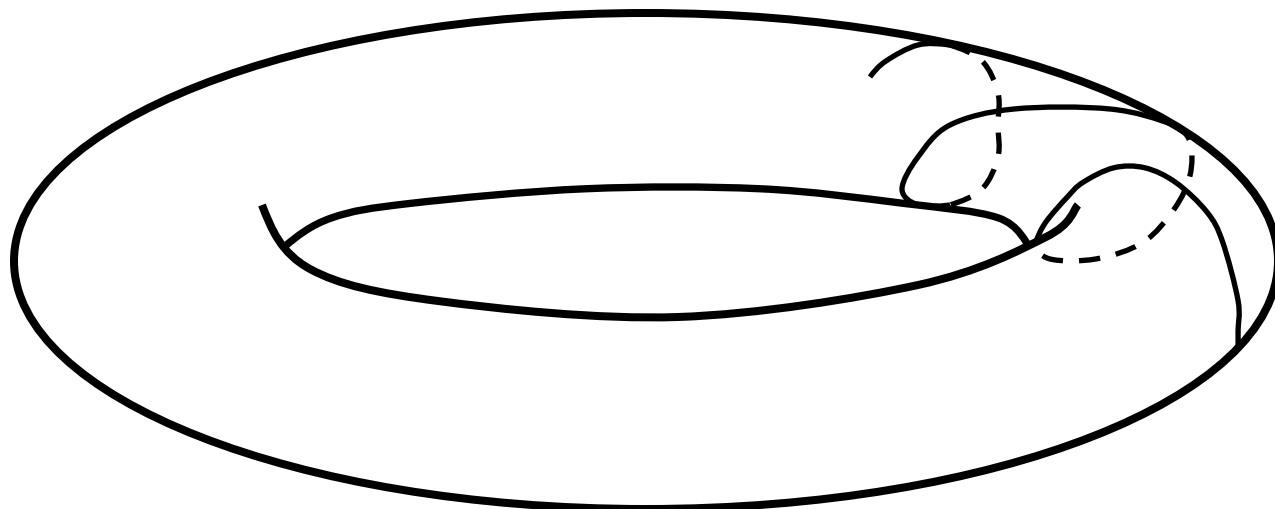


Behavior of the SALI for regular motion

Regular motion occurs on a torus and two different initial deviation vectors become tangent to the torus, generally having different directions.

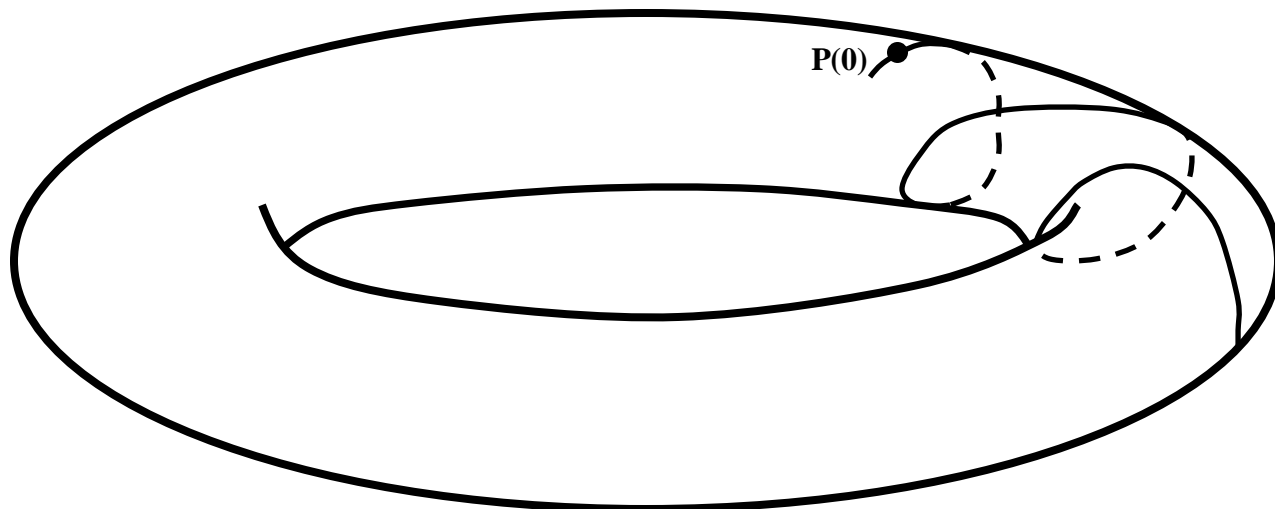
Behavior of the SALI for regular motion

Regular motion occurs on a torus and two different initial deviation vectors become tangent to the torus, generally having different directions.



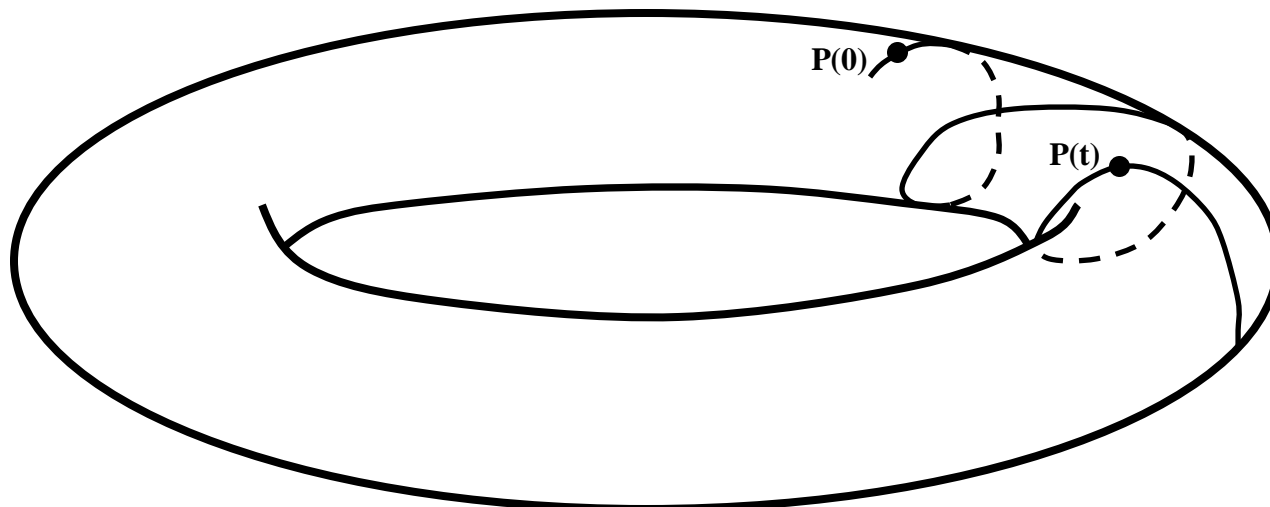
Behavior of the SALI for regular motion

Regular motion occurs on a torus and two different initial deviation vectors become tangent to the torus, generally having different directions.



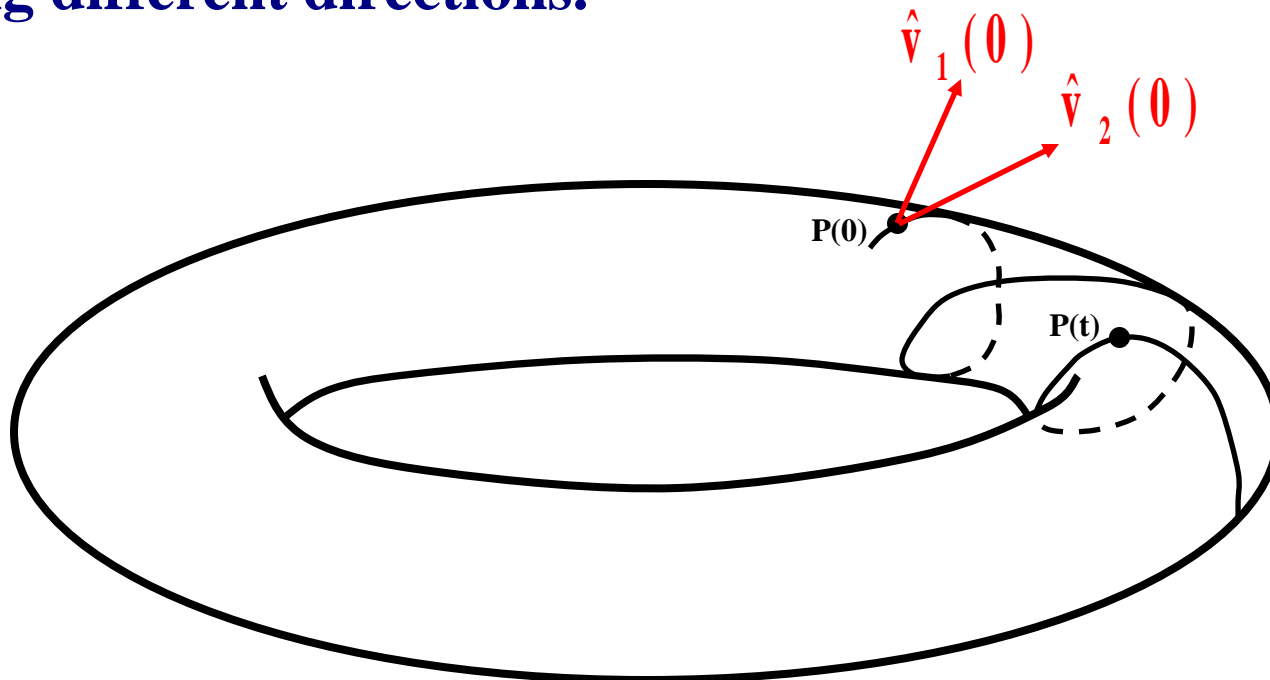
Behavior of the SALI for regular motion

Regular motion occurs on a torus and two different initial deviation vectors become tangent to the torus, generally having different directions.



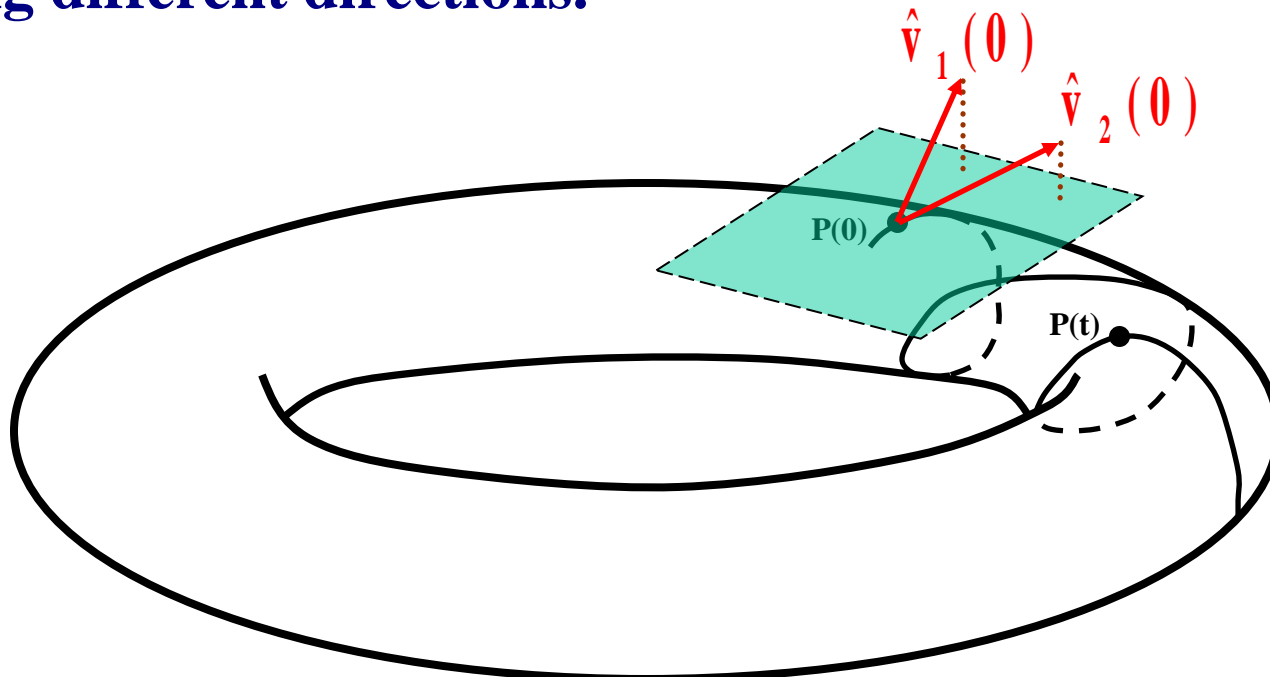
Behavior of the SALI for regular motion

Regular motion occurs on a torus and two different initial deviation vectors become tangent to the torus, generally having different directions.



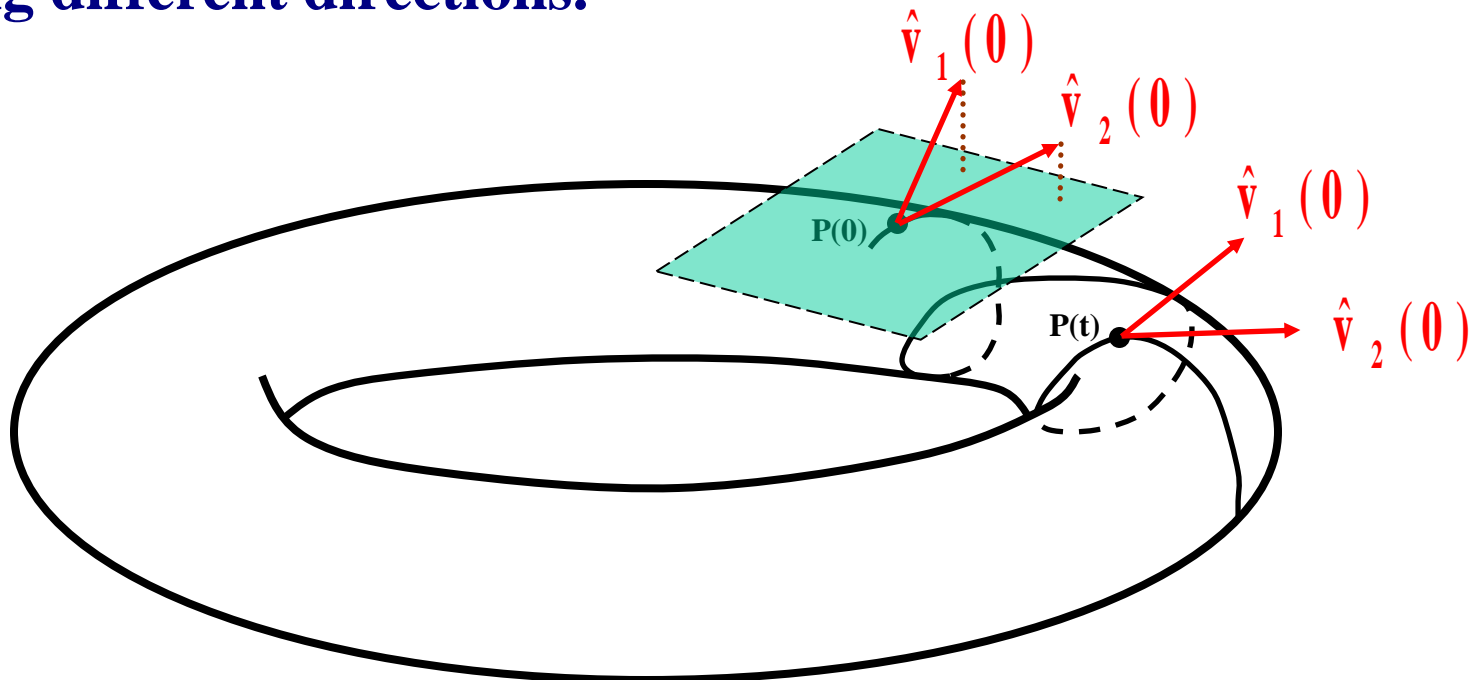
Behavior of the SALI for regular motion

Regular motion occurs on a torus and two different initial deviation vectors become tangent to the torus, generally having different directions.



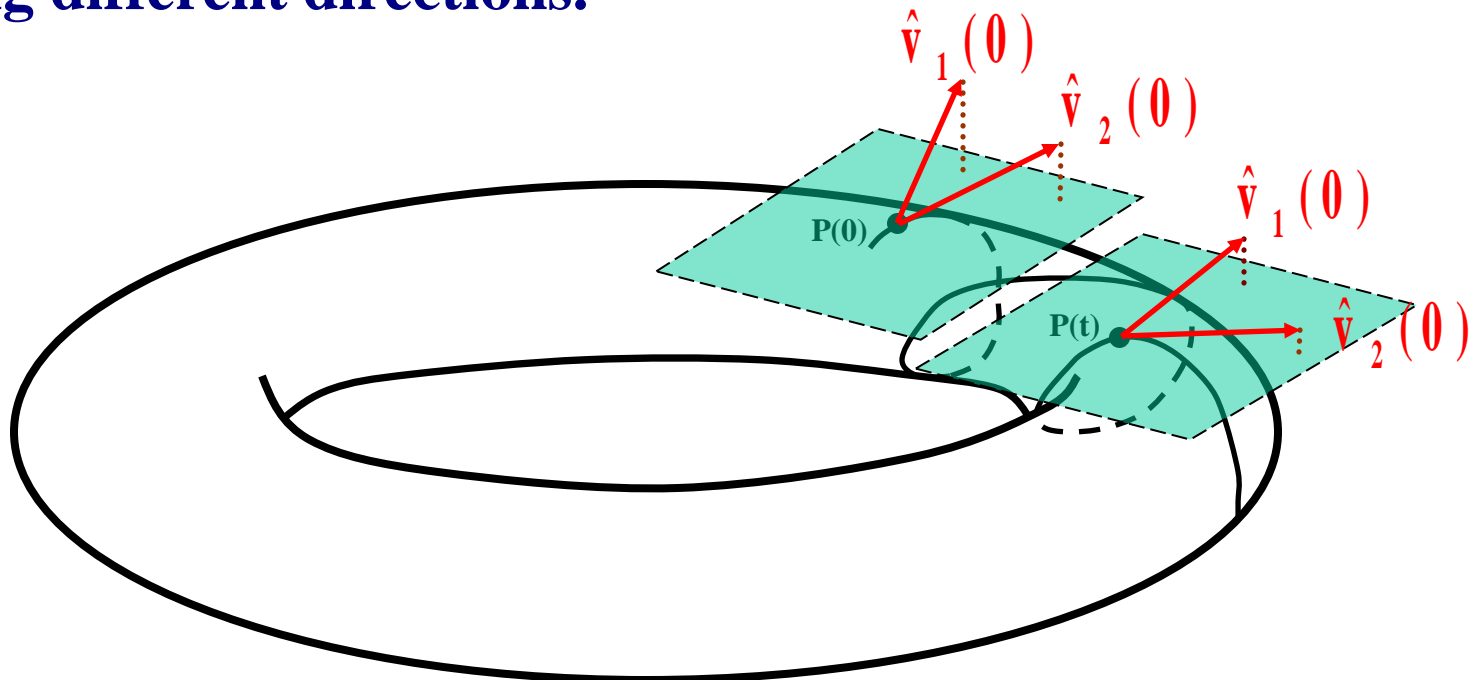
Behavior of the SALI for regular motion

Regular motion occurs on a torus and two different initial deviation vectors become tangent to the torus, generally having different directions.



Behavior of the SALI for regular motion

Regular motion occurs on a torus and two different initial deviation vectors become tangent to the torus, generally having different directions.



Applications – Hénon-Heiles system

As an example, we consider the 2D Hénon-Heiles system:

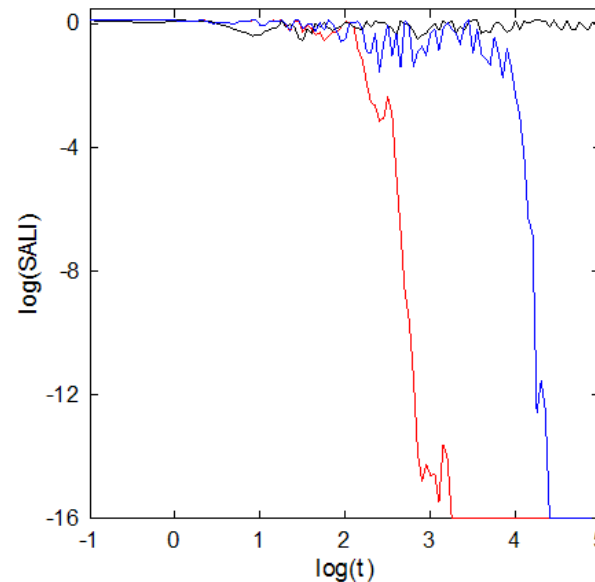
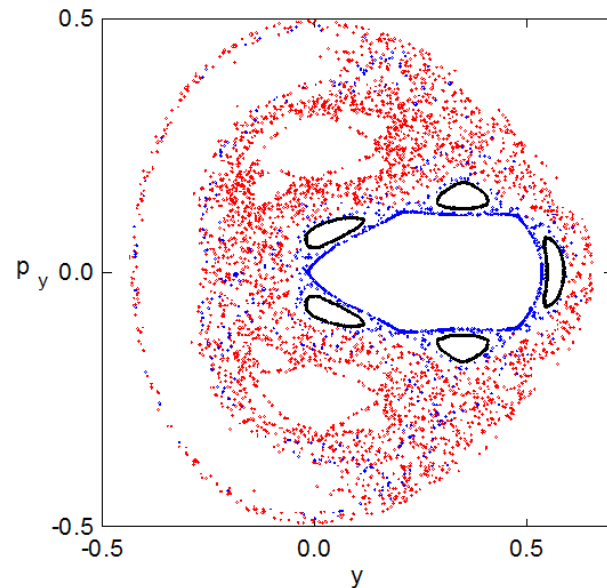
$$H_2 = \frac{1}{2}(p_x^2 + p_y^2) + \frac{1}{2}(x^2 + y^2) + x^2y - \frac{1}{3}y^3$$

For E=1/8 we consider the orbits with initial conditions:

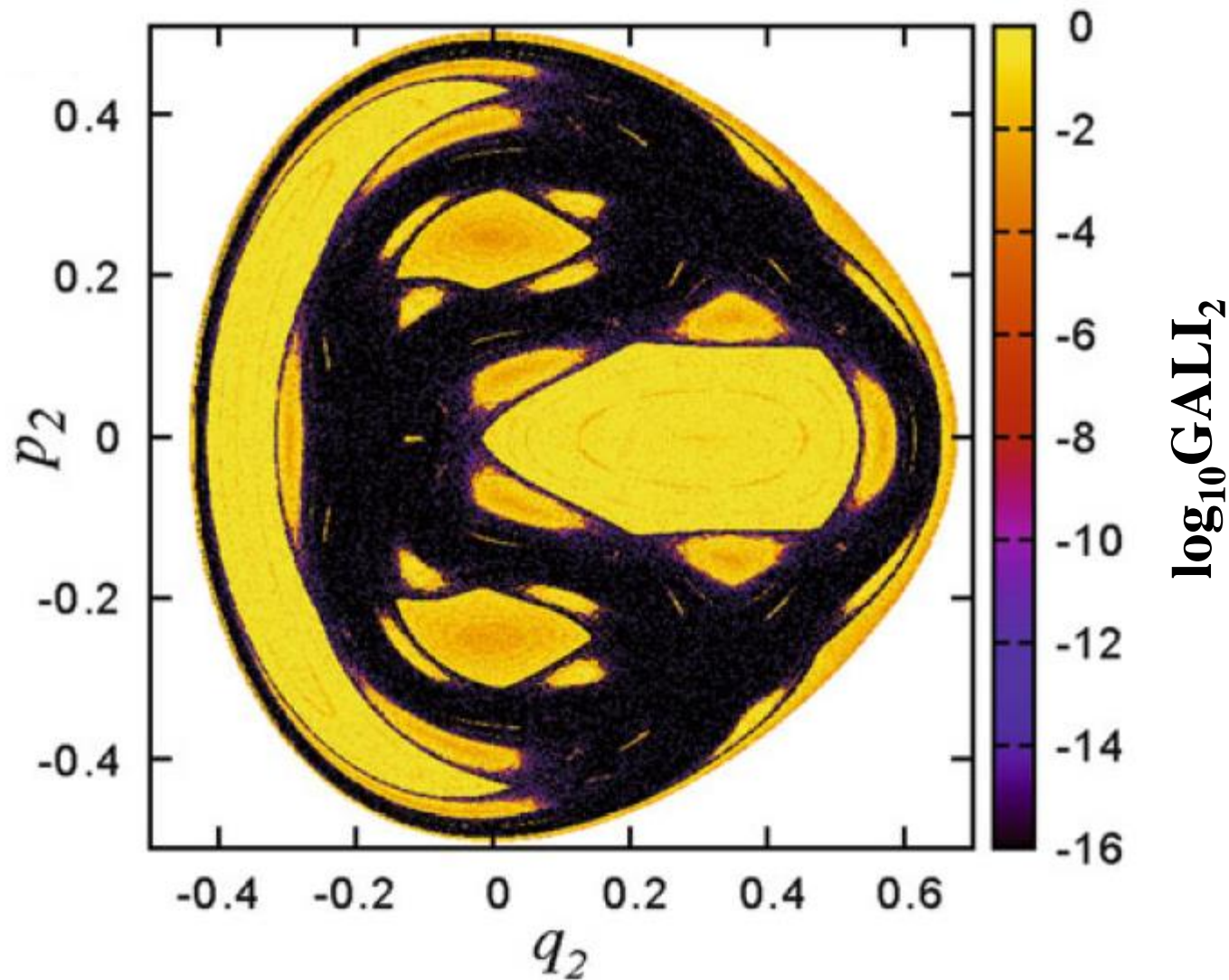
Regular orbit, $x=0$, $y=0.55$, $p_x=0.2417$, $p_y=0$

Chaotic orbit, $x=0$, $y=-0.016$, $p_x=0.49974$, $p_y=0$

Chaotic orbit, $x=0$, $y=-0.01344$, $p_x=0.49982$, $p_y=0$



Applications – Hénon-Heiles system



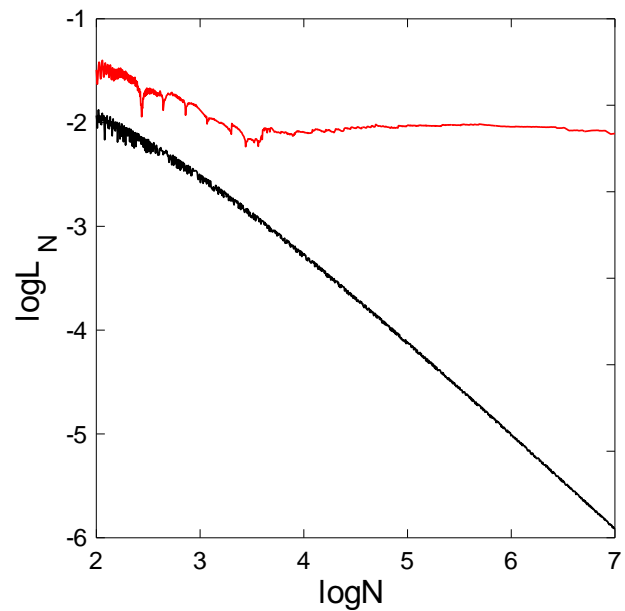
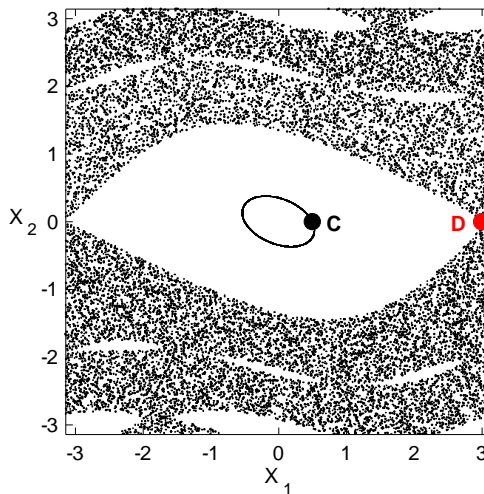
Applications – 4D map

$$\begin{aligned}
 \mathbf{x}'_1 &= \mathbf{x}_1 + \mathbf{x}_2 \\
 \mathbf{x}'_2 &= \mathbf{x}_2 - \nu \sin(\mathbf{x}_1 + \mathbf{x}_2) - \mu [1 - \cos(\mathbf{x}_1 + \mathbf{x}_2 + \mathbf{x}_3 + \mathbf{x}_4)] \quad (\text{mod } 2\pi) \\
 \mathbf{x}'_3 &= \mathbf{x}_3 + \mathbf{x}_4 \\
 \mathbf{x}'_4 &= \mathbf{x}_4 - \kappa \sin(\mathbf{x}_3 + \mathbf{x}_4) - \mu [1 - \cos(\mathbf{x}_1 + \mathbf{x}_2 + \mathbf{x}_3 + \mathbf{x}_4)]
 \end{aligned}$$

For $\nu=0.5$, $\kappa=0.1$, $\mu=0.1$ we consider the orbits:

regular orbit C with initial conditions $x_1=0.5$, $x_2=0$, $x_3=0.5$, $x_4=0$.

chaotic orbit D with initial conditions $x_1=3$, $x_2=0$, $x_3=0.5$, $x_4=0$.



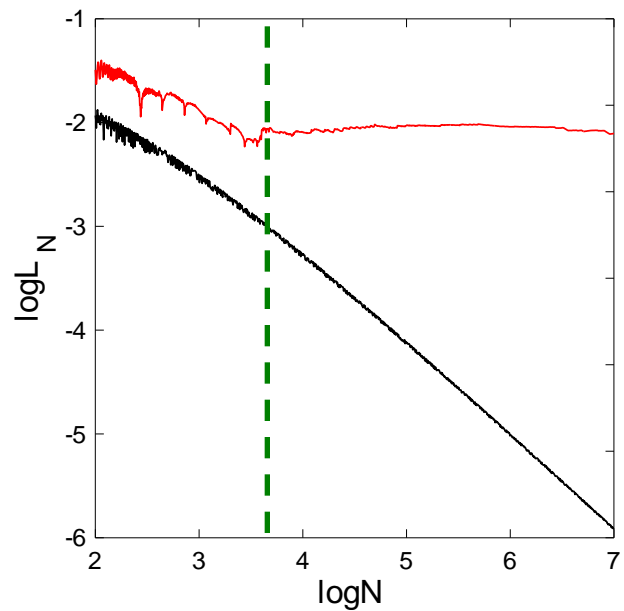
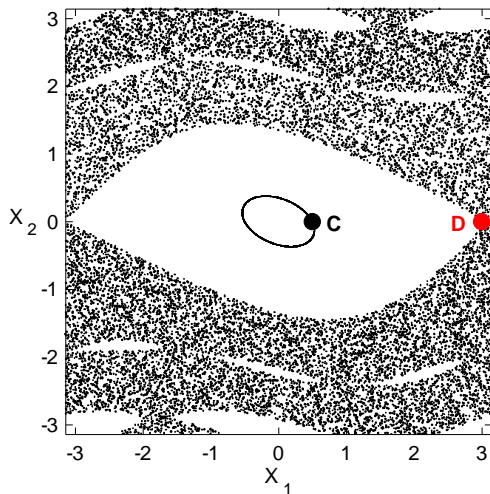
Applications – 4D map

$$\begin{aligned}
 \mathbf{x}'_1 &= \mathbf{x}_1 + \mathbf{x}_2 \\
 \mathbf{x}'_2 &= \mathbf{x}_2 - v \sin(\mathbf{x}_1 + \mathbf{x}_2) - \mu [1 - \cos(\mathbf{x}_1 + \mathbf{x}_2 + \mathbf{x}_3 + \mathbf{x}_4)] \quad (\text{mod } 2\pi) \\
 \mathbf{x}'_3 &= \mathbf{x}_3 + \mathbf{x}_4 \\
 \mathbf{x}'_4 &= \mathbf{x}_4 - \kappa \sin(\mathbf{x}_3 + \mathbf{x}_4) - \mu [1 - \cos(\mathbf{x}_1 + \mathbf{x}_2 + \mathbf{x}_3 + \mathbf{x}_4)]
 \end{aligned}$$

For $v=0.5$, $\kappa=0.1$, $\mu=0.1$ we consider the orbits:

regular orbit C with initial conditions $x_1=0.5$, $x_2=0$, $x_3=0.5$, $x_4=0$.

chaotic orbit D with initial conditions $x_1=3$, $x_2=0$, $x_3=0.5$, $x_4=0$.



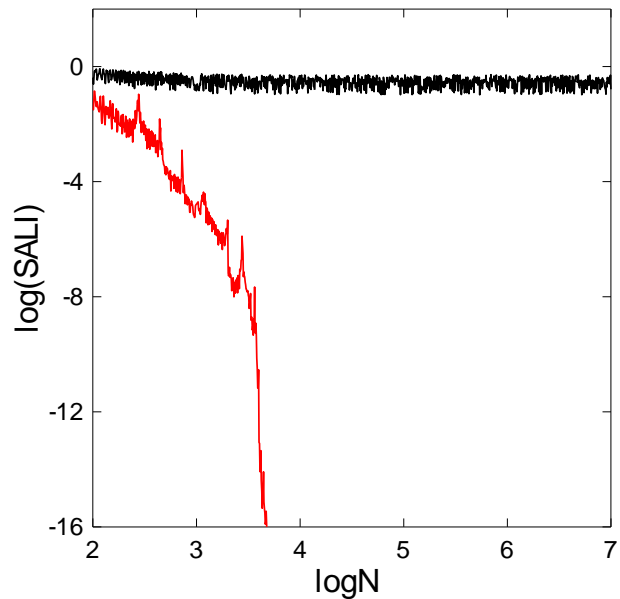
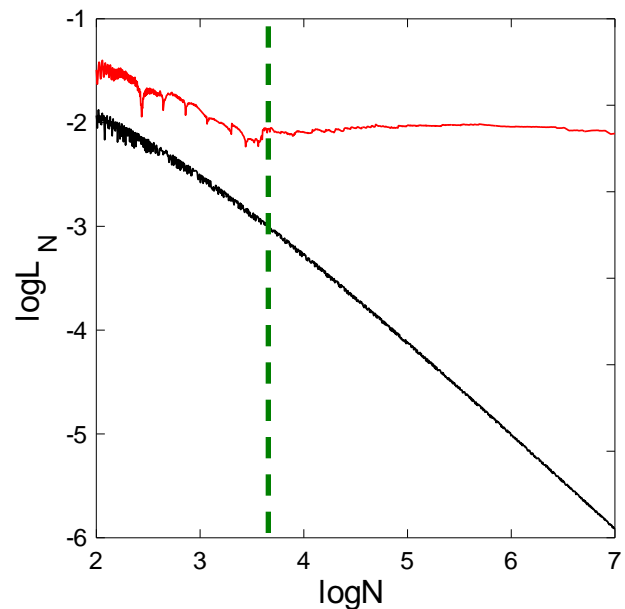
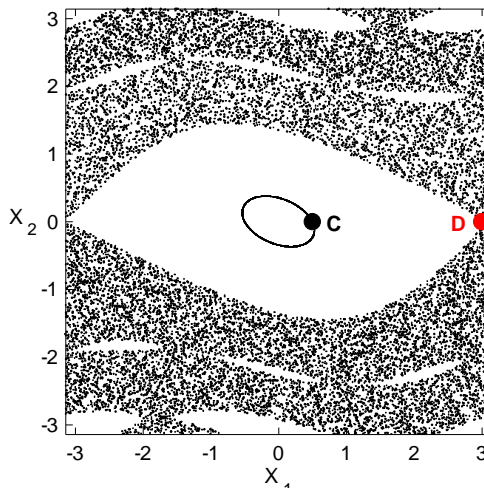
Applications – 4D map

$$\begin{aligned}
 \mathbf{x}'_1 &= \mathbf{x}_1 + \mathbf{x}_2 \\
 \mathbf{x}'_2 &= \mathbf{x}_2 - v \sin(\mathbf{x}_1 + \mathbf{x}_2) - \mu [1 - \cos(\mathbf{x}_1 + \mathbf{x}_2 + \mathbf{x}_3 + \mathbf{x}_4)] \quad (\text{mod } 2\pi) \\
 \mathbf{x}'_3 &= \mathbf{x}_3 + \mathbf{x}_4 \\
 \mathbf{x}'_4 &= \mathbf{x}_4 - \kappa \sin(\mathbf{x}_3 + \mathbf{x}_4) - \mu [1 - \cos(\mathbf{x}_1 + \mathbf{x}_2 + \mathbf{x}_3 + \mathbf{x}_4)]
 \end{aligned}$$

For $v=0.5$, $\kappa=0.1$, $\mu=0.1$ we consider the orbits:

regular orbit C with initial conditions $x_1=0.5$, $x_2=0$, $x_3=0.5$, $x_4=0$.

chaotic orbit D with initial conditions $x_1=3$, $x_2=0$, $x_3=0.5$, $x_4=0$.



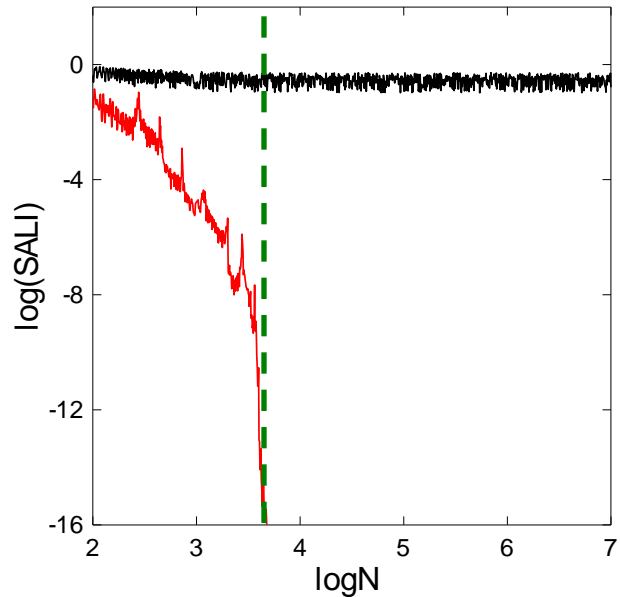
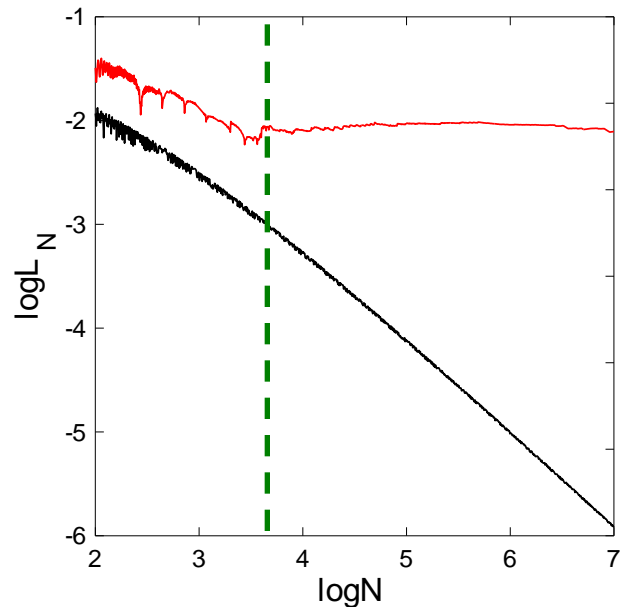
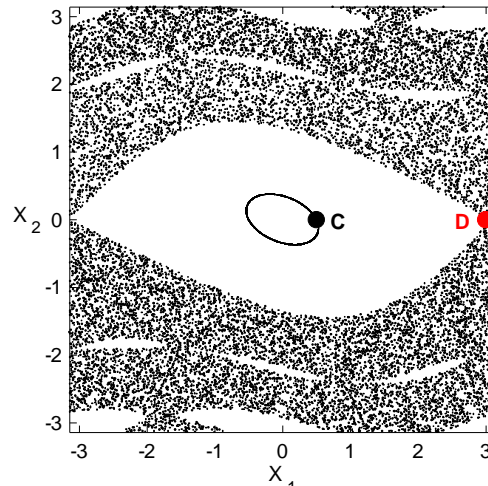
Applications – 4D map

$$\begin{aligned}
 \mathbf{x}'_1 &= \mathbf{x}_1 + \mathbf{x}_2 \\
 \mathbf{x}'_2 &= \mathbf{x}_2 - v \sin(\mathbf{x}_1 + \mathbf{x}_2) - \mu [1 - \cos(\mathbf{x}_1 + \mathbf{x}_2 + \mathbf{x}_3 + \mathbf{x}_4)] \quad (\text{mod } 2\pi) \\
 \mathbf{x}'_3 &= \mathbf{x}_3 + \mathbf{x}_4 \\
 \mathbf{x}'_4 &= \mathbf{x}_4 - \kappa \sin(\mathbf{x}_3 + \mathbf{x}_4) - \mu [1 - \cos(\mathbf{x}_1 + \mathbf{x}_2 + \mathbf{x}_3 + \mathbf{x}_4)]
 \end{aligned}$$

For $v=0.5$, $\kappa=0.1$, $\mu=0.1$ we consider the orbits:

regular orbit C with initial conditions $x_1=0.5$, $x_2=0$, $x_3=0.5$, $x_4=0$.

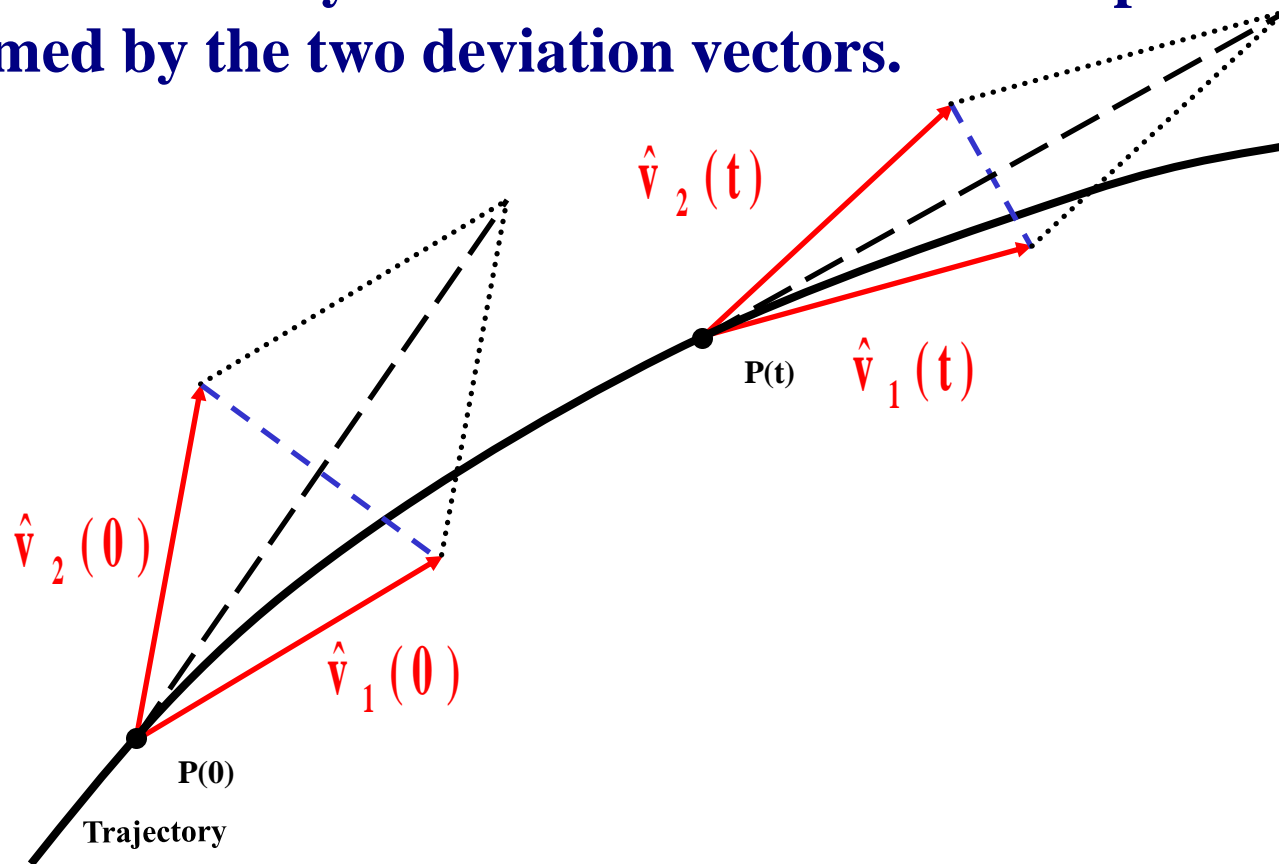
chaotic orbit D with initial conditions $x_1=3$, $x_2=0$, $x_3=0.5$, $x_4=0$.



The
Generalized ALignment Indices
(GALIs)
method

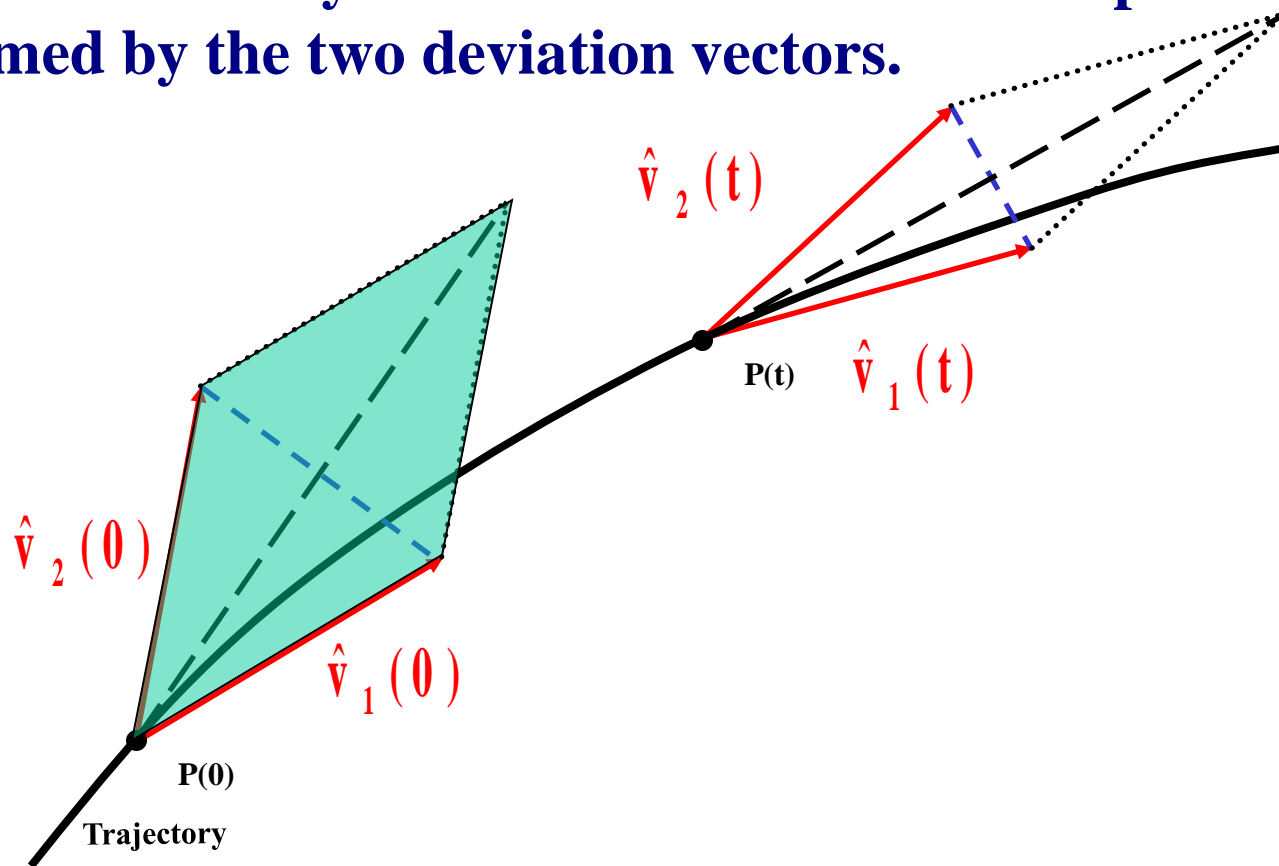
Definition of the Generalized Alignment Index (GALI)

SALI effectively measures the ‘area’ of the parallelogram formed by the two deviation vectors.



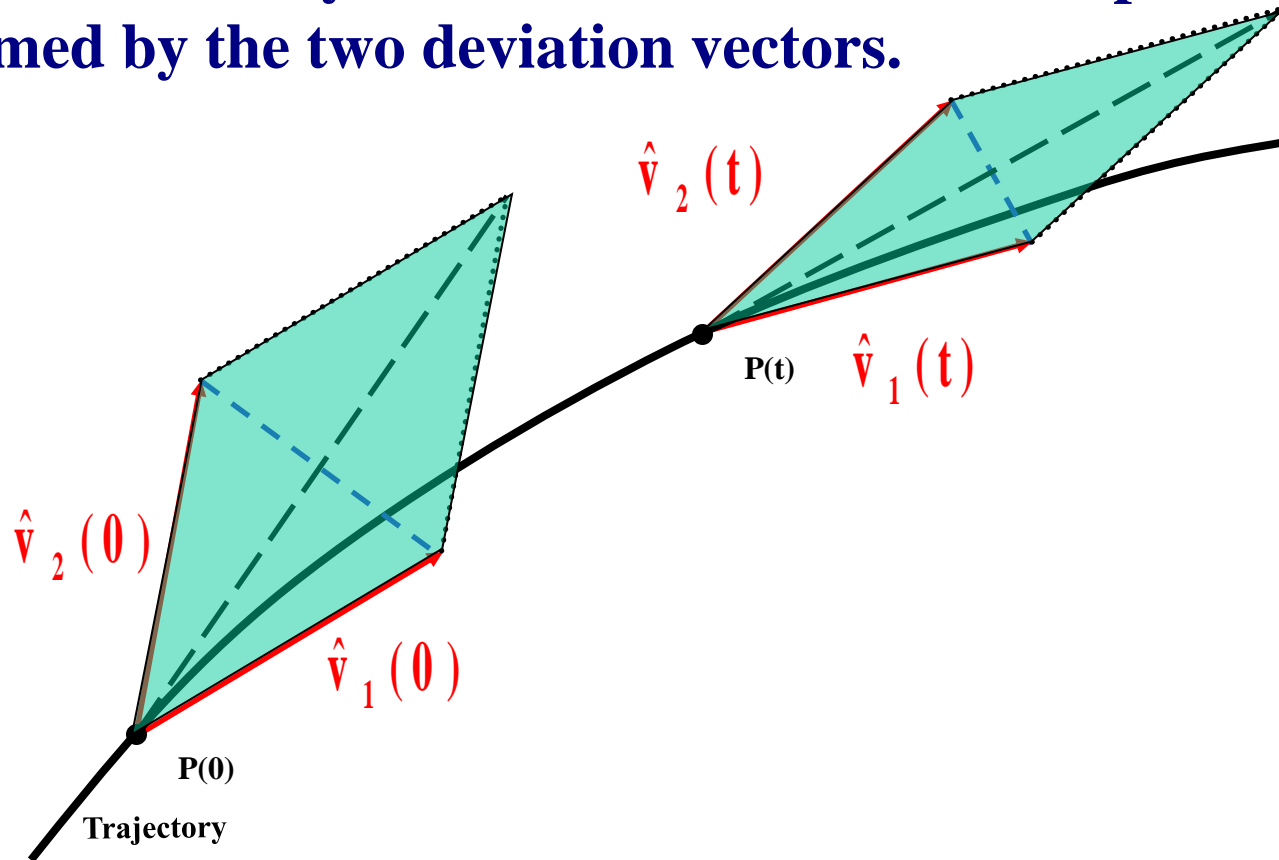
Definition of the Generalized Alignment Index (GALI)

SALI effectively measures the ‘area’ of the parallelogram formed by the two deviation vectors.



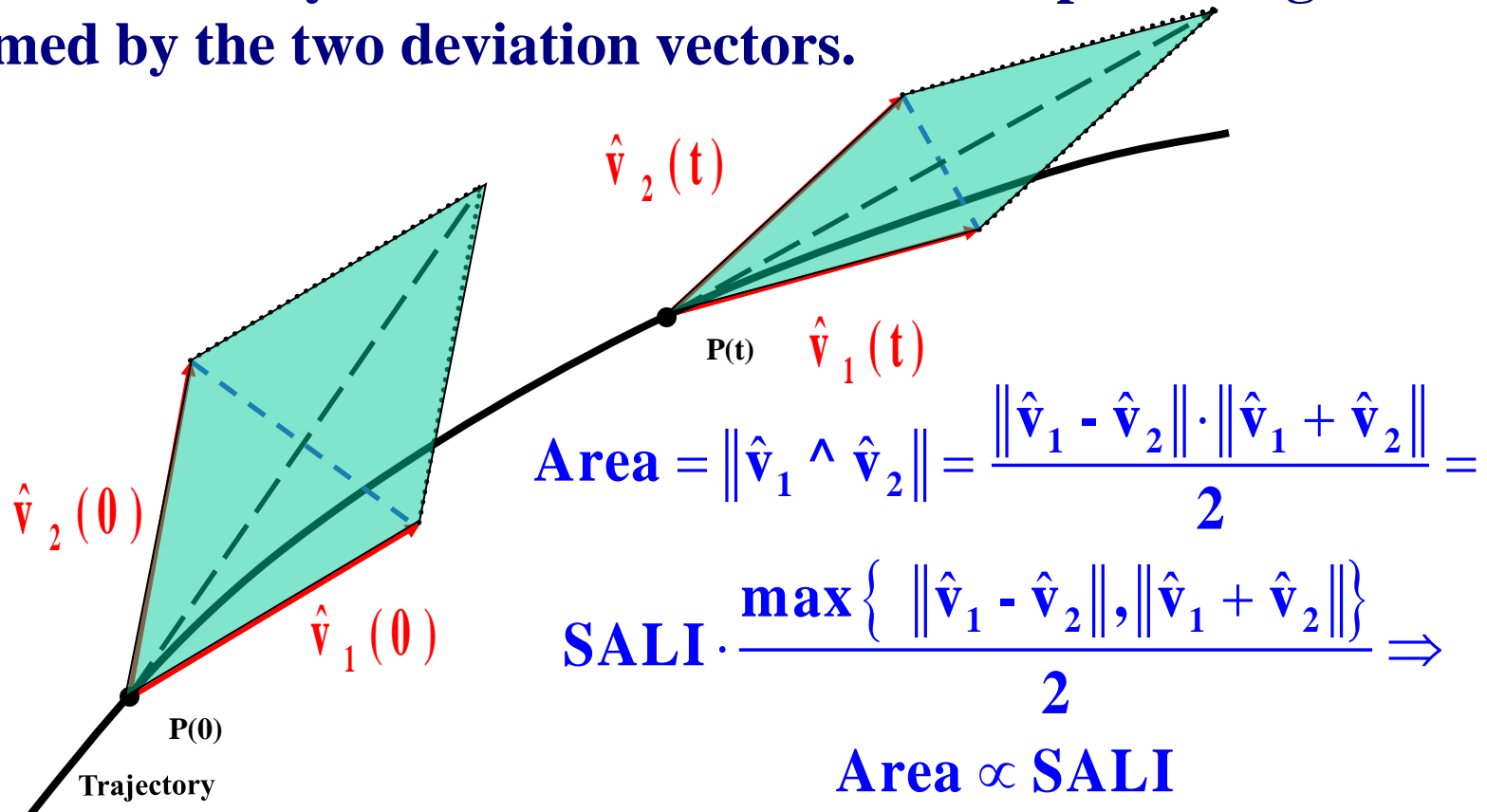
Definition of the Generalized Alignment Index (GALI)

SALI effectively measures the ‘area’ of the parallelogram formed by the two deviation vectors.



Definition of the Generalized Alignment Index (GALI)

SALI effectively measures the ‘area’ of the parallelogram formed by the two deviation vectors.



Definition of the GALI

In the case of an N degree of freedom Hamiltonian system or a $2N$ symplectic map we follow the evolution of

k deviation vectors with $2 \leq k \leq 2N$,

and define (Ch.S., Bountis, Antonopoulos, 2007, Physica D) the Generalized Alignment Index (GALI) of order k :

$$G A L I_k(t) = \left\| \hat{v}_1(t) \wedge \hat{v}_2(t) \wedge \dots \wedge \hat{v}_k(t) \right\|$$

where

$$\hat{v}_1(t) = \frac{v_1(t)}{\|v_1(t)\|}$$

Behavior of the GALI_k for chaotic motion

GALI_k ($2 \leq k \leq 2N$) tends exponentially to zero with exponents that involve the values of the first k largest Lyapunov exponents $\sigma_1, \sigma_2, \dots, \sigma_k$:

$$\text{GALI}_k(t) \propto e^{-[(\sigma_1 + \sigma_2) + (\sigma_1 + \sigma_3) + \dots + (\sigma_1 + \sigma_k)]t}$$

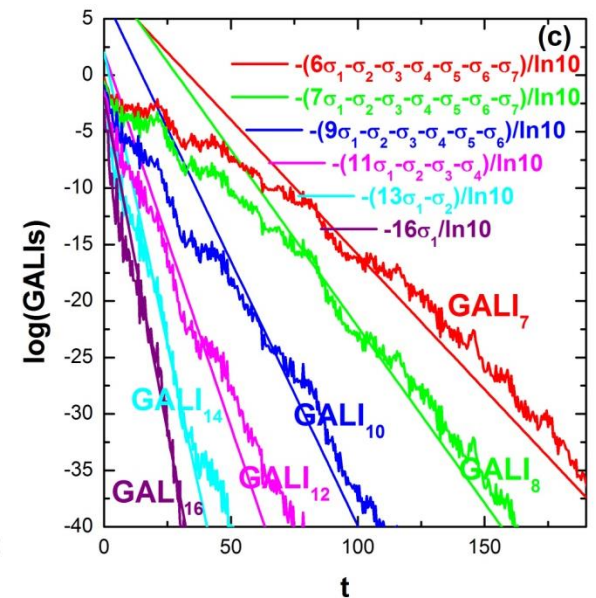
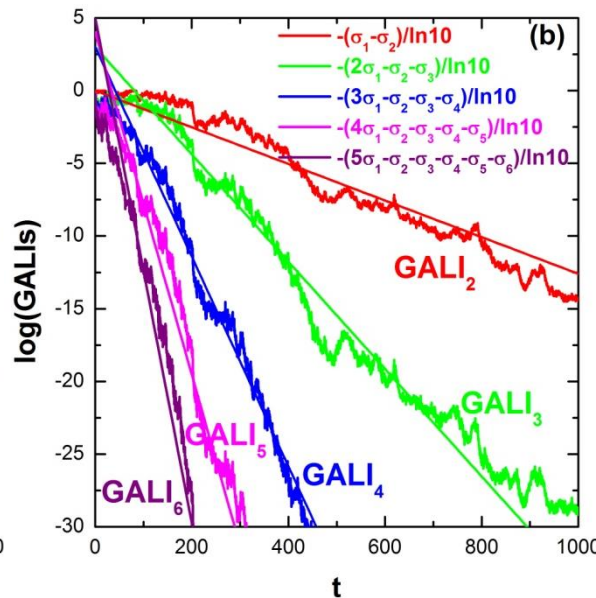
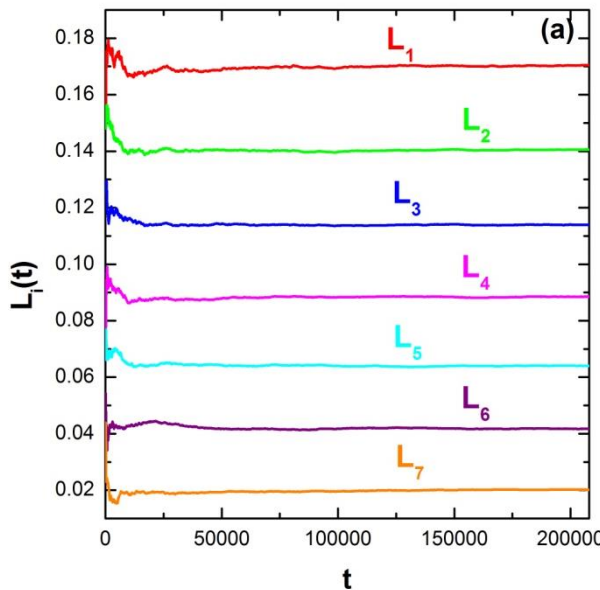
The above relation is valid even if some Lyapunov exponents are equal, or very close to each other.

Behavior of the GALI_k for chaotic motion

N particles Fermi-Pasta-Ulam (FPU) system:

$$H = \frac{1}{2} \sum_{i=1}^N p_i^2 + \sum_{i=0}^N \left[\frac{1}{2} (q_{i+1} - q_i)^2 + \frac{\beta}{4} (q_{i+1} - q_i)^4 \right]$$

with fixed boundary conditions, N=8 and $\beta=1.5$.



Behavior of the GALI_k for regular motion

If the motion occurs on an s -dimensional torus with $s \leq N$ then the behavior of GALI_k is given by (Ch.S., Bountis, Antonopoulos, 2008, Eur. Phys. J. Sp. Top.):

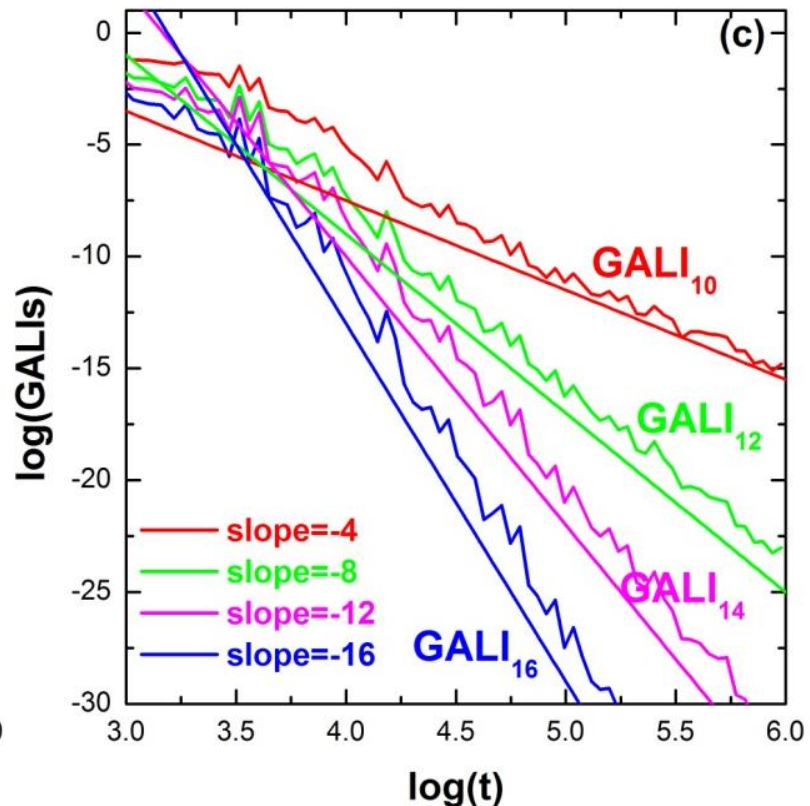
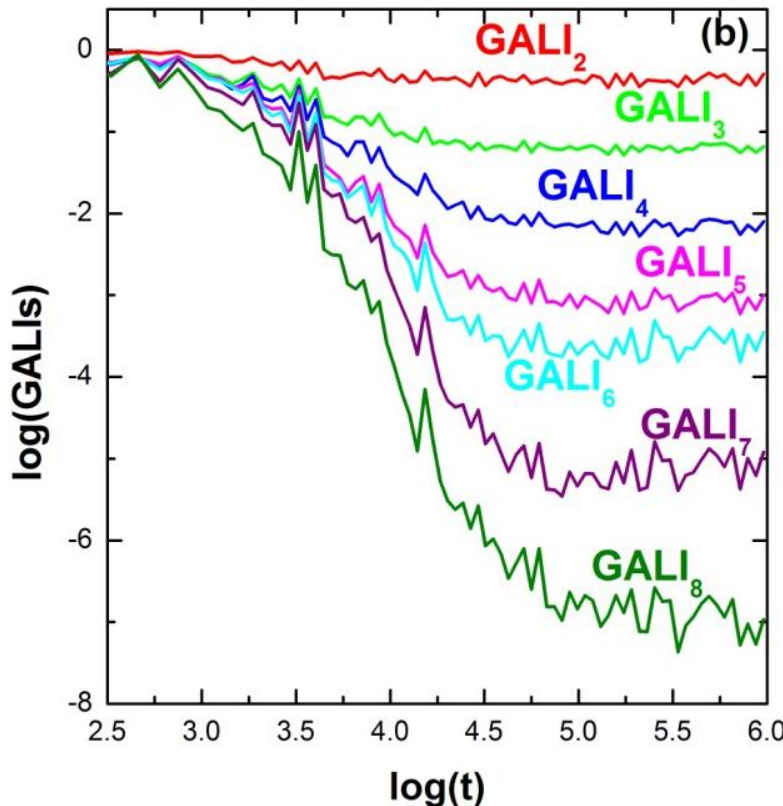
$$\text{GALI}_k(t) \propto \begin{cases} \text{constant} & \text{if } 2 \leq k \leq s \\ \frac{1}{t^{k-s}} & \text{if } s < k \leq 2N - s \\ \frac{1}{t^{2(k-N)}} & \text{if } 2N - s < k \leq 2N \end{cases}$$

while in the common case with $s=N$ we have :

$$\text{GALI}_k(t) \propto \begin{cases} \text{constant} & \text{if } 2 \leq k \leq N \\ \frac{1}{t^{2(k-N)}} & \text{if } N < k \leq 2N \end{cases}$$

Behavior of the GALI_k for regular motion

N=8 FPU system



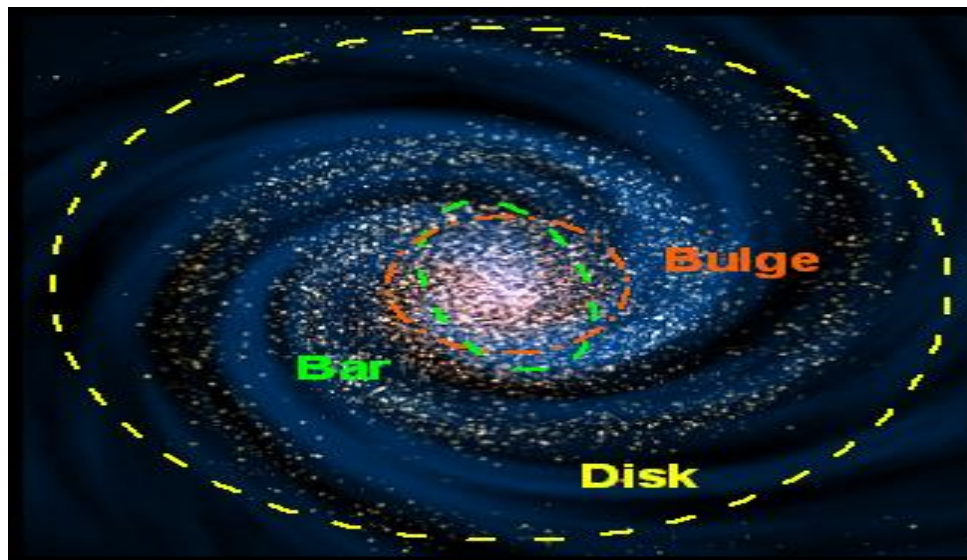
A time-dependent Hamiltonian system

Barred galaxies

NGC 1433



NGC 2217



Barred galaxy model

The 3D bar rotates around its short z -axis (x : long axis and y : intermediate). The Hamiltonian that describes the motion for this model is:

$$H = \frac{1}{2}(p_x^2 + p_y^2 + p_z^2) + V(x, y, z) - \Omega_b(xp_y - yp_x) \equiv Energy$$

This model consists of the superposition of potentials describing an **axisymmetric** part and a **bar** component of the galaxy (Manos, Bountis, Ch.S., 2013, J. Phys. A).

a) Axisymmetric component:

i) **Plummer sphere:**

$$V_{sphere}(x, y, z) = -\frac{GM_s}{\sqrt{x^2 + y^2 + z^2 + \epsilon_s^2}}$$

ii) **Miyamoto–Nagai disc:**

$$V_{disc}(x, y, z) = -\frac{GM_d}{\sqrt{x^2 + y^2 + (A + \sqrt{B^2 + z^2})^2}}$$

b) **Bar component:** $V_{bar}(x, y, z) = -\pi Gabc \frac{\rho_c}{n+1} \int_{\lambda}^{\infty} \frac{du}{\Delta(u)} (1 - m^2(u))^{n+1},$

(**Ferrers bar**)

$$\boxed{\rho_c = \frac{105}{32\pi} \frac{GM_B}{abc}}$$

$$\text{where } m^2(u) = \frac{x^2}{a^2 + u} + \frac{y^2}{b^2 + u} + \frac{z^2}{c^2 + u}, \quad \Delta^2(u) = (a^2 + u)(b^2 + u)(c^2 + u),$$

n : positive integer ($n = 2$ for our model), λ : the unique positive solution of $m^2(\lambda) = 1$

Its density is:

$$\rho = \begin{cases} \rho_c (1 - m^2)^n, & \text{for } m \leq 1 \\ 0, & \text{for } m > 1 \end{cases}, \quad \text{where } m^2 = \frac{x^2}{a^2} + \frac{y^2}{b^2} + \frac{z^2}{c^2}, \quad a > b > c \text{ and } n = 2.$$

Time-dependent barred galaxy model

The 3D bar rotates around its short z -axis (x : long axis and y : intermediate). The Hamiltonian that describes the motion for this model is:

$$H = \frac{1}{2}(p_x^2 + p_y^2 + p_z^2) + V(x, y, z, t) - \Omega_b(xp_y - yp_x) \equiv Energy$$

This model consists of the superposition of potentials describing an **axisymmetric** part and a **bar** component of the galaxy (Manos, Bountis, Ch.S., 2013, J. Phys. A).

a) **Axisymmetric component:**

$$M_S + M_B(t) + M_D(t) = 1, \text{ with } M_B(t) = M_B(0) + \alpha t$$

i) **Plummer sphere:**

$$V_{sphere}(x, y, z) = -\frac{GM_S}{\sqrt{x^2 + y^2 + z^2 + \varepsilon_s^2}}$$

ii) **Miyamoto–Nagai disc:**

$$V_{disc}(x, y, z) = -\frac{GM_D(t)}{\sqrt{x^2 + y^2 + (A + \sqrt{B^2 + z^2})^2}}$$

b) **Bar component:** $V_{bar}(x, y, z) = -\pi Gabc \frac{\rho_c}{n+1} \int_{\lambda}^{\infty} \frac{du}{\Delta(u)} (1 - m^2(u))^{n+1},$

(Ferrers bar)

$$\rho_c = \frac{105}{32\pi} \frac{GM_B(t)}{abc}$$

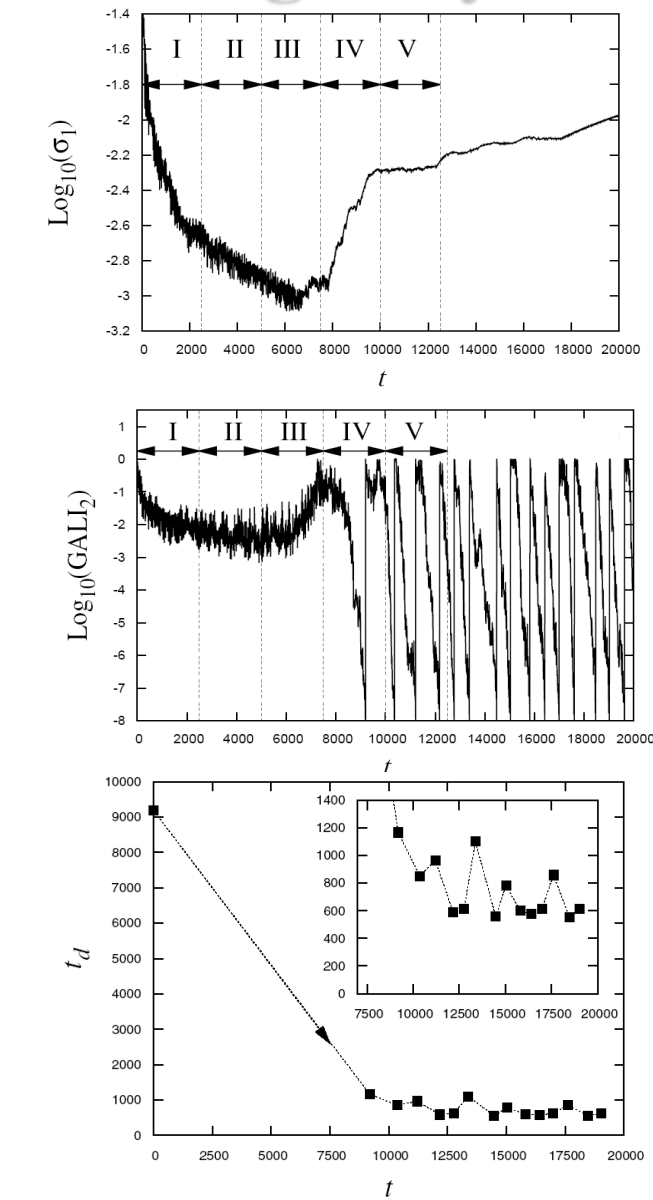
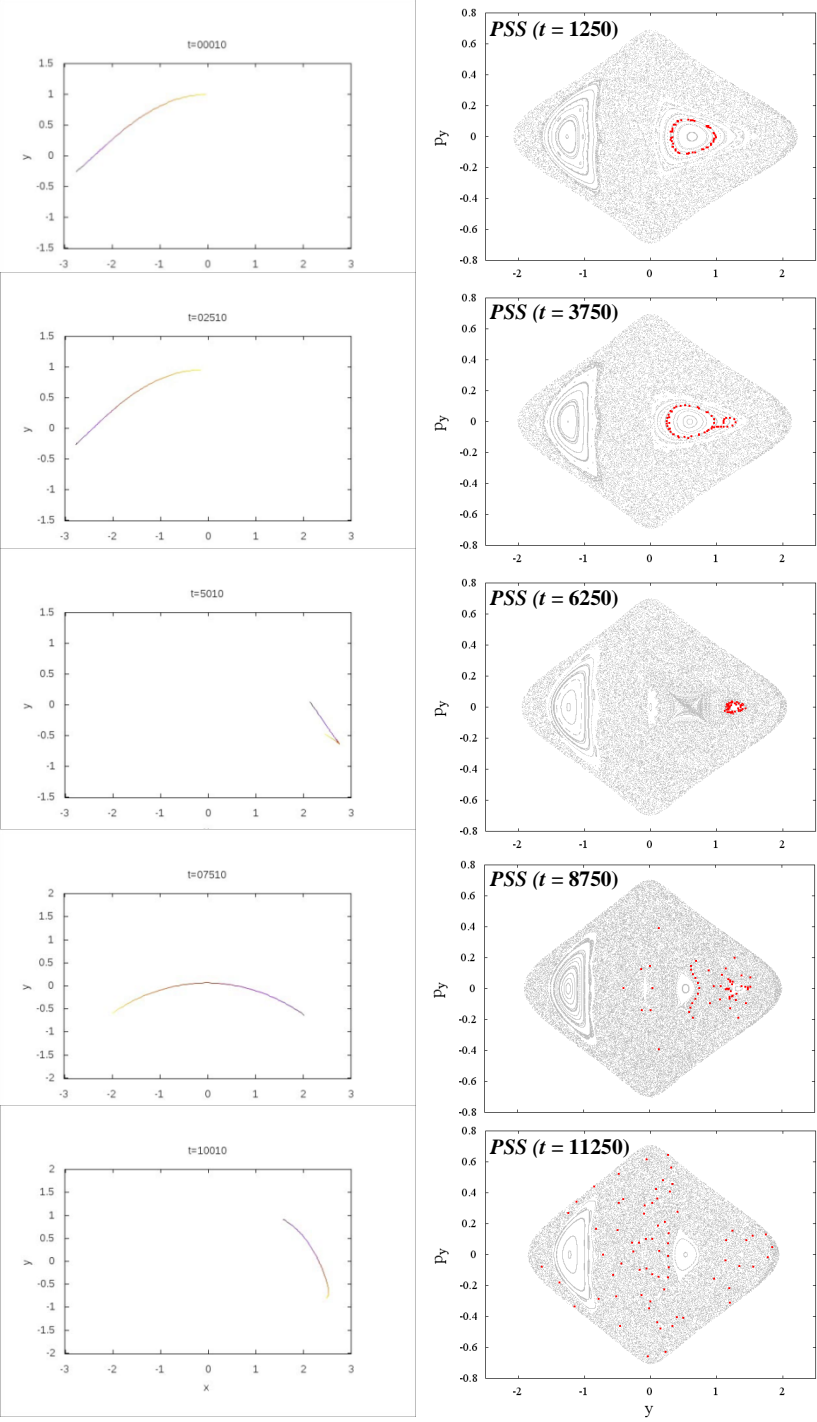
$$\text{where } m^2(u) = \frac{x^2}{a^2 + u} + \frac{y^2}{b^2 + u} + \frac{z^2}{c^2 + u}, \Delta^2(u) = (a^2 + u)(b^2 + u)(c^2 + u),$$

n : positive integer ($n = 2$ for our model), λ : the unique positive solution of $m^2(\lambda) = 1$

Its density is:

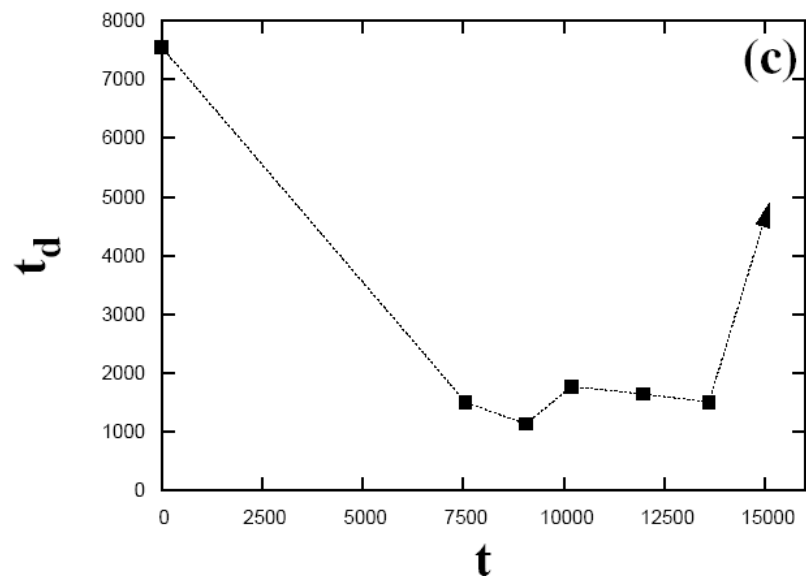
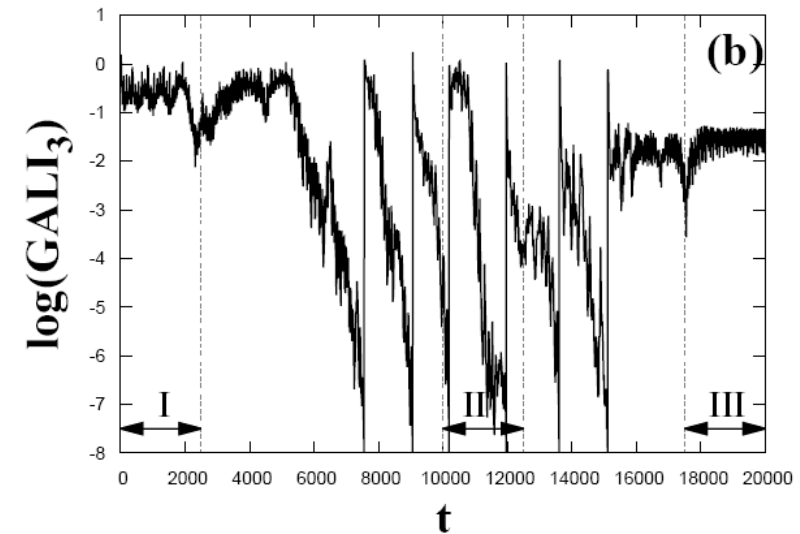
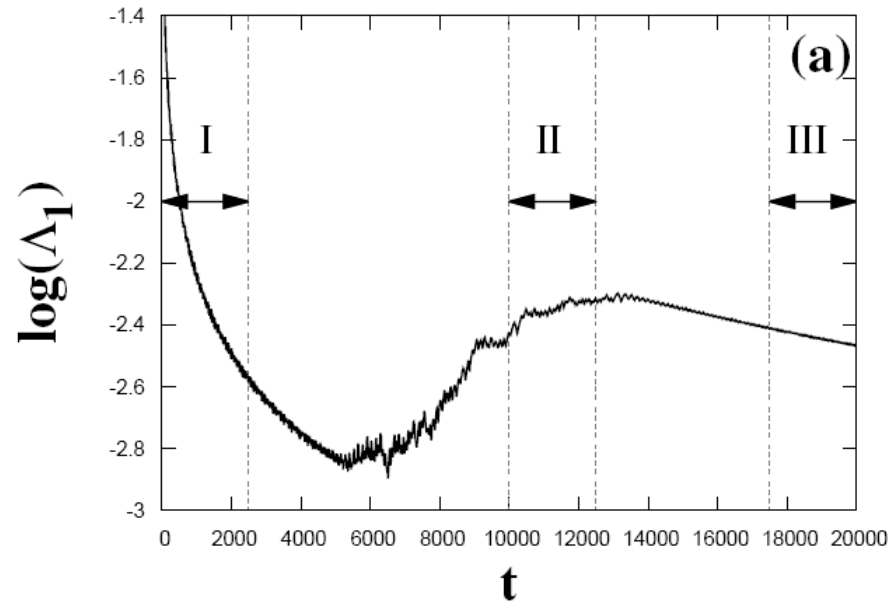
$$\rho = \begin{cases} \rho_c (1 - m^2)^n, & \text{for } m \leq 1 \\ 0, & \text{for } m > 1 \end{cases}, \text{ where } m^2 = \frac{x^2}{a^2} + \frac{y^2}{b^2} + \frac{z^2}{c^2}, a > b > c \text{ and } n = 2.$$

Time-dependent 2D barred galaxy model



Time-dependent 3D barred galaxy model

Interplay between chaotic and regular motion



Summary

- We discussed methods of chaos detection based on
 - ✓ the visualization of orbits
 - ✓ the numerical analysis of orbits
 - ✓ the evolution of deviation vectors (variational equations – tangent map)
- The Smaller (SALI) and the Generalized (GALI) ALignment Index methods are **fast, efficient and easy to compute** chaos indicator.
- Behaviour of the Generalized ALignment Index of order k (GALI_k):
 - ✓ Chaotic motion: it tends exponentially to zero
 - ✓ Regular motion: it fluctuates around non-zero values (or goes to zero following power-laws)
- GALI_k indices :
 - ✓ can distinguish rapidly and with certainty between regular and chaotic motion
 - ✓ can be used to characterize individual orbits as well as "chart" chaotic and regular domains in phase space
 - ✓ can identify regular motion on low-dimensional tori
 - ✓ are perfectly suited for studying the global dynamics of multidimentonal systems, as well as of time-dependent models

Main References I

- **The color and rotation (CR) method**
 - ✓ Patsis P. A. & Zachilas L (1994) *Int. J. Bif. Chaos*, **4**, 1399
 - ✓ Katsanikas M & Patsis P A (2011) *Int. J. Bif. Chaos*, **21**, 467
 - ✓ Katsanikas M, Patsis P A & Contopoulos G. (2011) *Int. J. Bif. Chaos*, **21**, 2321
- **the 3D phase space slices (3PSS) technique**
 - ✓ Richter M, Lange S, Backer A & Ketzmerick R (2014), *Phys. Rev. E* **89**, 022902
 - ✓ Lange S, Richter M, Onken F, Backer A & Ketzmerick R (2014), *Chaos* **24**, 024409
 - ✓ Onken F, Lange S, Ketzmerick R & Backer A (2016), *Chaos* **26**, 063124
- **Frequency Analysis**
 - ✓ Laskar J (1990) *Icarus*, **88**, 266
 - ✓ Laskar J, Froeschle C & Celletti A (1992) *Physica D*, **56**, 253
 - ✓ Laskar J (1993) *Physica D*, **67**, 257
 - ✓ Bartolini R, Bazzani A, Giovannozzi M, Scandale W & Todesco E (1996) *Part. Accel.* **52**, 147
 - ✓ Laskar J (1999) in *Hamiltonian systems with three or more degrees of freedom* (ed. Simo C / Plenum Press) p 134
- **Lyapunov exponents**
 - ✓ Oseledec V I (1968) *Trans. Moscow Math. Soc.*, **19**, 197
 - ✓ Benettin G, Galgani L, Giorgilli A & Strelcyn J-M (1980) *Meccanica*, March, 9
 - ✓ Benettin G, Galgani L, Giorgilli A & Strelcyn J-M (1980) *Meccanica*, March, 21
 - ✓ Wolf A, Swift J B, Swinney H L & Vastano J A (1985) *Physica D*, **16**, 285
 - ✓ Ch.S. (2010) *Lect. Notes Phys.*, **790**, 63

Main References II

- **0-1 test**
 - ✓ Gottwald G A & Melbourne I (2004) Proc. R. Soc. A, **460**, 603
 - ✓ Gottwald G A & Melbourne I (2005) Physica D, **212**, 100
 - ✓ Gottwald G A & Melbourne I (2009) SIAM J. Appl. Dyn., **8**, 129
 - ✓ Gottwald G A & Melbourne I (2016) Lect. Notes Phys., **915**, 221
- **FLI – OFLI – OFLI2**
 - ✓ Froeschle C, Lega E & Gonczi R (1997) Celest. Mech. Dyn. Astron., **67**, 41
 - ✓ Guzzo M, Lega E & Froeschle C (2002) Physica D, **163**, 1
 - ✓ Fouchard M, Lega E, Froeschle C & Froeschle C (2002) Celest. Mech. Dyn. Astron., **83**, 205
 - ✓ Barrio R (2005) Chaos Sol. Fract., **25**, 71
 - ✓ Barrio R (2006) Int. J. Bif. Chaos, **16**, 2777
 - ✓ Lega E, Guzzo M & Froeschle C (2016) Lect. Notes Phys., **915**, 35
 - ✓ Barrio R (2016) Lect. Notes Phys., **915**, 55
- **MEGNO**
 - ✓ Cincotta P M & Simo (2000) Astron. Astroph. Suppl. Ser., **147**, 205
 - ✓ Cincotta P M, Giordano C M & Simo C (2003) Physica D, **182**, 151
 - ✓ Cincotta P M, & Giordano C M (2016) Lect. Notes Phys., **915**, 93
- **RLI**
 - ✓ Sandor Zs, Erdi B & Efthymiopoulos C (2000) Celest. Mech. Dyn. Astron., **78**, 113
 - ✓ Sandor Zs, Erdi B, Szell A & Funk B (2004) Celest. Mech. Dyn. Astron., **90** 127
 - ✓ Sandor Zs & Maffione N (2016) Lect. Notes Phys., **915**, 183

Main References III

- **SALI**
 - ✓ Ch.S. (2001) *J. Phys. A*, **34**, 10029
 - ✓ Ch.S., Antonopoulos Ch, Bountis T C & Vrahatis M N (2003) *Prog. Theor. Phys. Supp.*, **150**, 439
 - ✓ Ch.S., Antonopoulos Ch, Bountis T C & Vrahatis M N (2004) *J. Phys. A*, **37**, 6269
 - ✓ Bountis T & Ch.S. (2006) *Nucl. Inst Meth. Phys Res. A*, **561**, 173
 - ✓ Boreaux J, Carletti T, Ch.S. & Vittot M (2012) *Com. Nonlin. Sci. Num. Sim.*, **17**, 1725
 - ✓ Boreaux J, Carletti T, Ch.S., Papaphilippou Y & Vittot M (2012) *Int. J. Bif. Chaos*, **22**, 1250219
- **GALI**
 - ✓ Ch.S., Bountis T C & Antonopoulos Ch (2007) *Physica D*, **231**, 30
 - ✓ Ch.S., Bountis T C & Antonopoulos Ch (2008) *Eur. Phys. J. Sp. Top.*, **165**, 5
 - ✓ Gerlach E, Eggl S & Ch.S. (2012) *Int. J. Bif. Chaos*, **22**, 1250216
 - ✓ Manos T, Ch.S. & Antonopoulos Ch (2012) *Int. J. Bif. Chaos*, **22**, 1250218
 - ✓ Manos T, Bountis T & Ch.S. (2013) *J. Phys. A*, **46**, 254017
- **Reviews on SALI and GALI**
 - ✓ Bountis T C & Ch.S. (2012) ‘Complex Hamiltonian Dynamics’, Chapter 5, Springer Series in Synergetics
 - ✓ Ch.S. & Manos T (2016) *Lect. Notes Phys.*, **915**, 129